

## RESEARCH ARTICLE SUMMARY

## CYTOSKELETON

# Severing enzymes amplify microtubule arrays through lattice GTP-tubulin incorporation

Annapurna Vemu, Ewa Szczesna, Elena A. Zehr, Jeffrey O. Spector, Nikolaus Grigorieff, Alexandra M. Deaconescu, Antonina Roll-Mecak\*

**INTRODUCTION:** The microtubule cytoskeleton is continuously sculpted by polymerization, depolymerization, cross-linking, and microtubule severing. Microtubule severing generates internal breaks in microtubules through a poorly understood mechanism. It is mediated by the AAA [adenosine triphosphatases (ATPases) associated with various cellular activities] ATPases katanin, spastin, and fidgetin. Paradoxically, despite the destructive activity of severing enzymes, loss of severing enzyme activity leads to a decrease rather than an increase in microtubule mass. It was hypothesized that this severing enzyme-dependent increase in microtubule mass results from templated nucleation from the severed ends. This is an attractive hypothesis for a mechanism to generate microtubule mass, especially in the absence of centrosome-based nucleation as in neurons or meiotic spindles. However, for this amplification to operate, the guanosine diphosphate (GDP)-tubulin lattice exposed through

severing would have to be stabilized. The GDP-microtubule lattice is the product of guanosine triphosphate (GTP)-tubulin polymerization and depolymerizes spontaneously when exposed in the absence of a stabilizing GTP cap. We examined this paradox by examining the effects of the severing enzymes spastin and katanin on microtubule structure and dynamics in vitro.

**RATIONALE:** Because light microscopy-based severing assays fail to capture ultrastructural features of severing intermediates due to resolution limitations, we used negative-stain transmission electron microscopy (TEM) to capture and image spastin- and katanin-mediated microtubule severing in vitro. We combined these experiments with quantitative analyses of tubulin and microtubule polymer dynamics by using total internal reflection fluorescence (TIRF) microscopy to understand the effects of severing on microtubule networks.

**RESULTS:** Our electron microscopy analyses coupled with TIRF microscopy revealed that spastin and katanin actively extract tubulin dimers out of the microtubule, introducing nanoscale damage along the microtubule, and that this action is counteracted by spontaneous, de novo incorporation of GTP-tubulin dimers from the soluble pool. Depending on the local balance between the rates of active tubulin extraction and passive repair, there are two

## ON OUR WEBSITE

Read the full article at <http://dx.doi.org/10.1126/science.aau1504>

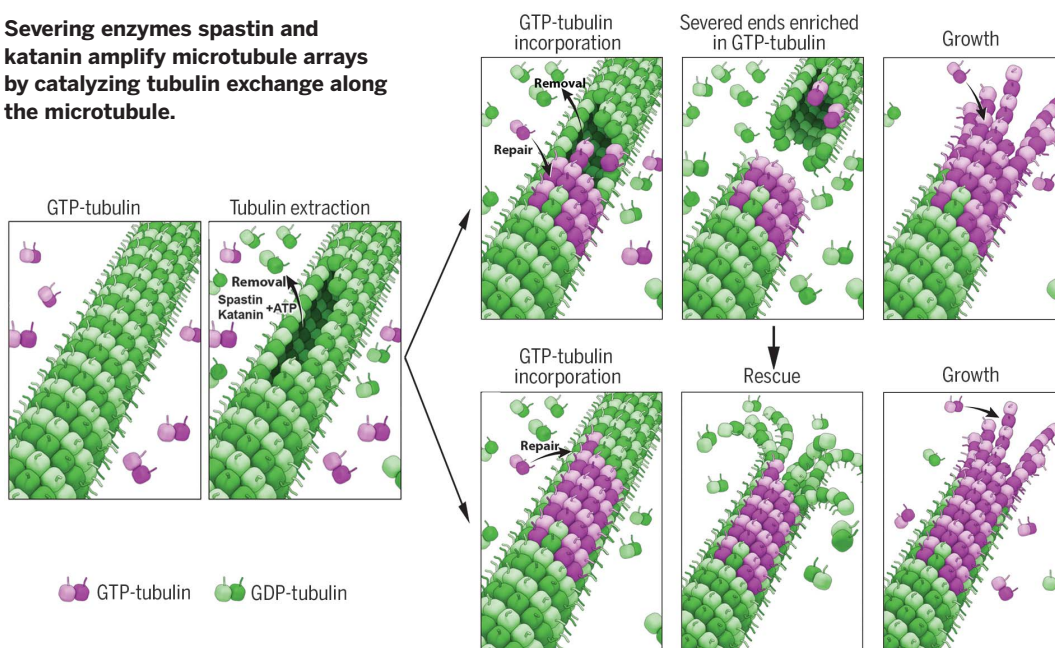
non-mutually exclusive consequences: The microtubule is rejuvenated with GTP-tubulin islands that stabilize it against depolymerization, or severing proceeds to completion

and the newly severed microtubule ends emerge with a high density of stabilizing GTP-tubulin. Consistent with this, we found that spastin and katanin activities increase rates of microtubule rescue and that rescues occur preferentially at sites of enzyme-dependent GTP-tubulin incorporation. Lastly and unexpectedly, we found that the incorporation of GTP-tubulin at severing sites ensures that the newly severed plus ends are stable because they emerge with a high density of GTP-tubulin that protects them against spontaneous depolymerization and promotes elongation. The synergy between the increased rescue rates and the stabilization of the newly severed ends leads to microtubule amplification.

**CONCLUSION:** Our study identifies the microtubule-severing enzymes spastin and katanin as biological agents that introduce GTP-tubulin islands within microtubules and demonstrates that microtubule-severing enzymes alone can amplify microtubule number and mass

by promoting GTP-tubulin incorporation into the microtubule shaft, away from the dynamic ends long thought to be the sole locus of tubulin exchange. This microtubule-based amplification mechanism in the absence of a nucleating factor helps explain why the loss of spastin and katanin results in the loss of microtubule mass in systems that are dependent on noncentrosomal microtubule generation. ■

**Severing enzymes spastin and katanin amplify microtubule arrays by catalyzing tubulin exchange along the microtubule.**



The list of author affiliations is available in the full article online.

\*Corresponding author. Email: [antonina@mail.nih.gov](mailto:antonina@mail.nih.gov)  
Cite this article as A. Vemu et al., *Science* 361, eaau1504 (2018).  
DOI: 10.1126/science.aau1504

## RESEARCH ARTICLE

## CYTOSKELETON

# Severing enzymes amplify microtubule arrays through lattice GTP-tubulin incorporation

Annapurna Vemu<sup>1\*</sup>, Ewa Szczesna<sup>1\*</sup>, Elena A. Zehr<sup>1</sup>, Jeffrey O. Spector<sup>1</sup>, Nikolaus Grigorieff<sup>2,†</sup>, Alexandra M. Deaconescu<sup>3</sup>, Antonina Roll-Mecak<sup>1,4,‡</sup>

Spastin and katanin sever and destabilize microtubules. Paradoxically, despite their destructive activity they increase microtubule mass *in vivo*. We combined single-molecule total internal reflection fluorescence microscopy and electron microscopy to show that the elemental step in microtubule severing is the generation of nanoscale damage throughout the microtubule by active extraction of tubulin heterodimers. These damage sites are repaired spontaneously by guanosine triphosphate (GTP)-tubulin incorporation, which rejuvenates and stabilizes the microtubule shaft. Consequently, spastin and katanin increase microtubule rescue rates. Furthermore, newly severed ends emerge with a high density of GTP-tubulin that protects them against depolymerization. The stabilization of the newly severed plus ends and the higher rescue frequency synergize to amplify microtubule number and mass. Thus, severing enzymes regulate microtubule architecture and dynamics by promoting GTP-tubulin incorporation within the microtubule shaft.

The plasticity of the microtubule cytoskeleton follows from multiple levels of regulation through microtubule-end polymerization and depolymerization, cross-linking, and microtubule severing. Microtubule severing generates internal breaks in microtubules. It is mediated by three enzymes of the AAA [adenosine triphosphatases (ATPases) associated with various cellular activities] ATPase family—katanin, spastin, and fidgetin [reviewed in (1)]—that are widely conserved in animals and plants. They are critical for the generation and maintenance of complex noncentrosomal microtubule arrays in neurons (2–5) and the plant cortex (6–8) and regulate meiotic and mitotic spindle morphology and length (9–12), ciliary biogenesis (13, 14), centriole duplication (14, 15), cytokinesis (16, 17), axonal growth (18), wound healing (19), and plant phototropism (7, 8). Both spastin and katanin are associated with debilitating diseases. Spastin is mutated in hereditary spastic paraplegias, neurodegenerative disorders characterized by lower-extremity weakness due to axonopathy [reviewed in (1)]. Katanin mutations

cause microcephaly, seizures, and severe developmental defects (14, 15, 20). Disease mutations impair microtubule severing (21, 22).

Paradoxically, in many of these systems, the loss of the microtubule-severing enzyme leads to a decrease in microtubule mass [reviewed in (1)]. Spastin loss causes sparse disorganized microtubule arrays in *Drosophila* synaptic boutons (2) and impaired axonal outgrowth and sparse microtubule arrays in zebra fish axons (23). Similarly, katanin loss leads to sparse cortical microtubule arrays in *Arabidopsis* (8, 24), whereas in *Caenorhabditis elegans* meiotic spindles, it results in the loss of microtubule mass and number (25). It was hypothesized that the observed increase in microtubule number and mass results from templated nucleation from the severed ends (26, 27). This is an attractive mechanism for rapidly generating microtubule mass, especially in the absence of centrosome-based nucleation as in neurons or meiotic spindles. This severing-dependent microtubule amplification has been directly observed in plant cortical microtubule arrays (8). However, for this amplification to operate, the guanosine diphosphate (GDP)-tubulin lattice exposed through severing would have to be stabilized because GDP-microtubules depolymerize spontaneously in the absence of a stabilizing guanosine triphosphate (GTP) cap (28–31). To study this paradox, we combined time-resolved transmission electron microscopy (TEM) and total internal reflection fluorescence (TIRF) microscopy to directly observe the effects of the severing enzymes spastin and katanin on microtubule structure and dynamics *in vitro*.

## Severing enzymes cause nanoscale damage to microtubules

Because light microscopy-based severing assays fail to capture ultrastructural features of severing intermediates due to resolution limitations, we used negative-stain TEM to capture and image spastin-mediated microtubule-severing intermediates *in vitro* with purified, recombinant spastin. To minimize severing-intermediate breakage, we performed severing reactions directly on electron microscopy (EM) grids. These on-grid reactions revealed a high density of “bites” into the protofilament structure (Fig. 1) that resulted in the removal of tubulin dimers. Severing reactions performed in a test tube with Taxol-stabilized microtubules that were then transferred to EM grids by pipetting produced many short microtubules with blunt ends (fig. S1A), similar to those previously reported *in vitro* with katanin (32), indicating that the fragile nanoscale-damaged severing intermediates are lost during pipetting. Thus, in our on-grid severing setup, we were able to capture intermediates that were otherwise disrupted by shear forces introduced by pipetting. Upon prolonged incubation (>5 min), severing was driven to completion on the EM grid, with severe destruction of the microtubule structure indicating that the intermediates observed were on pathway (fig. S1B). The nanoscale damage sites were observed with GDP-microtubules regardless of whether they were nonstabilized or stabilized with Taxol (Fig. 1, A and B). Similar observations were made with microtubules polymerized with the nonhydrolyzable analog guanylyl ( $\alpha,\beta$ -methylene diphosphonate (GMPCPP) (Fig. 1C). The nanoscale damage we observed *in vitro* is reminiscent of that observed by electron tomography in freeze-substituted *C. elegans* meiotic spindles (25). The same extraction of tubulin dimers and protofilament fraying were observed if reactions were performed in solution and then microtubules were deposited on an EM grid without pipetting to avoid shear (Fig. 1D and Materials and methods). In control reactions without the enzyme, the integrity of the lattice was preserved (fig. S1, C and D), whereas in the spastin-treated samples, nanoscale damage sites were detected every ~2.2  $\mu\text{m}$  (fig. S1D). Time-course experiments revealed a gradual increase in nanoscale damage, as well as in the number of shorter microtubules (Fig. 1E). We extended our TEM analyses to the microtubule-severing enzyme katanin (Fig. 1, F and G, and fig. S1, E to H). As with spastin, TEM revealed that katanin microtubule severing proceeds through progressive extraction of tubulin dimers out of the microtubule.

## Tubulin incorporation repairs nanoscale damage

Our TEM analysis showed that GMPCPP-microtubules, Taxol-stabilized microtubules, or nonstabilized microtubules do not sever even when peppered with spastin- and katanin-induced nanoscale damage and do not catastrophically depolymerize upon removal of the initial tubulin subunits. This raised the possibility that this damage could be repaired by incorporation of

<sup>1</sup>Cell Biology and Biophysics Unit, Porter Neuroscience Research Center, National Institute of Neurological Disorders and Stroke, Bethesda, MD 20892, USA. <sup>2</sup>Howard Hughes Medical Institute, Brandeis University, Waltham, MA 02454, USA. <sup>3</sup>Department of Molecular Biology, Cell Biology, and Biochemistry, Brown University, Providence, RI 02903, USA. <sup>4</sup>Biochemistry and Biophysics Center, National Heart, Lung, and Blood Institute, Bethesda, MD 20892, USA.

\*These authors contributed equally to this work.

†Present address: Janelia Farm Research Campus, Howard Hughes Medical Institute, Ashburn, VA 20147, USA.

‡Corresponding author. Email: antonina@mail.nih.gov

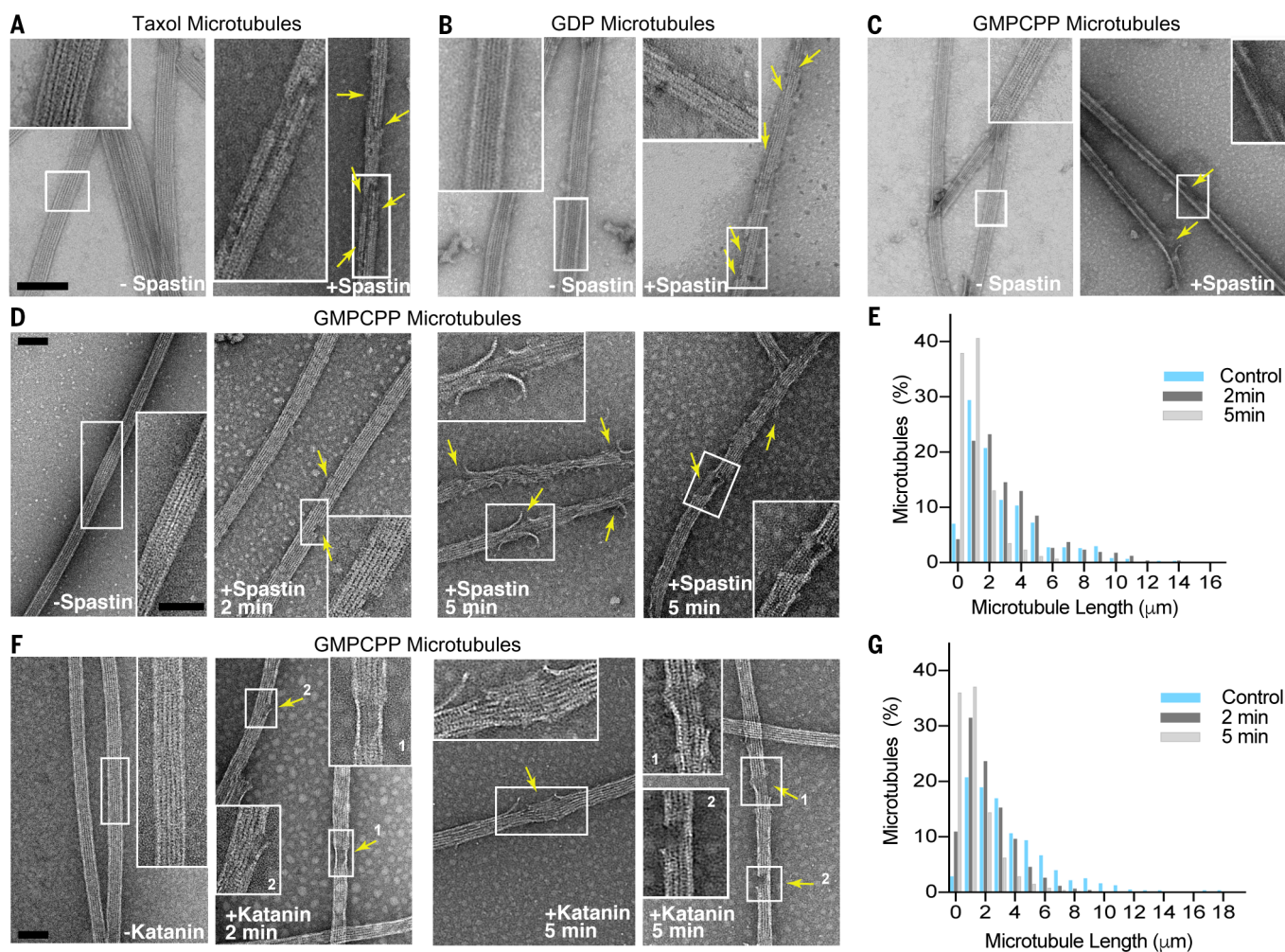


**Fig. 1. Spastin and katanin extract tubulin out of the microtubule.**

(A to C) Microtubules in the absence or presence of 33 nM spastin. The reaction proceeded on an EM grid for 1 min and was imaged by using negative-stain TEM (Materials and methods). Boxed regions are shown at 2 $\times$  magnification in insets. Microtubules were imaged at 30,000 $\times$  magnification. Arrows indicate nanoscale damage sites. Scale bar, 50 nm. (D) Fields of GMPCPP-microtubules incubated with buffer or 25 nM spastin. Severing proceeded in solution, and reaction mixtures

were passively deposited onto EM grids, negatively stained, and visualized by TEM (Materials and methods). Arrows indicate nanoscale damage. Microtubules were imaged at 13,000 $\times$  magnification; boxed regions are shown at 30,000 $\times$  magnification in insets. Scale bar, 50 nm. (E) Microtubule length distribution after incubation with spastin. (F) Fields of GMPCPP-microtubules incubated with buffer or 100 nM katanin and imaged as in (D). Scale bar, 50 nm. (G) Microtubule length distribution after incubation with katanin.

tubulin subunits from the soluble pool, as recently observed with mechanically damaged or photodamaged microtubules *in vitro* (33, 34). To test this hypothesis, we preassembled GMPCPP-microtubules fluorescently labeled with HiLyte 647 and incubated them with spastin (or katanin) and adenosine triphosphate (ATP) to initiate severing (Materials and methods). Under these conditions, we observed rare severing events (Fig. 2). Upon perfusion with soluble HiLyte 488-labeled tubulin and GTP, we observed tubulin incorporation in discrete patches along microtubules. These patches were numerous, far exceeding the number of severing events. Mock-treated microtubules showed no incorporation of tubulin into microtubules (Fig. 2, A to C). The tubulin concentration used was below the critical concentration for tubulin polymerization. Sim-

ilar results were obtained with Taxol-stabilized microtubules (fig. S2). Because photodamage can induce lattice defects in fluorescently labeled microtubules (34), we also performed experiments with unlabeled microtubules visualized by differential interference contrast (DIC) microscopy and also observed incorporation of tubulin into spastin-treated microtubules but not into controls (Fig. 2D).

In time-course experiments, both the number of repaired nanoscale damage sites and the mean fluorescence along repaired microtubules increased over time (figs. S3, A and B, and S4, A and B). The size of the repair sites [full width at half maximum (FWHM)] (figs. S3C and S4C) was initially diffraction limited and shifted toward larger values at longer incubation times, indicating an expansion of the damage as de-

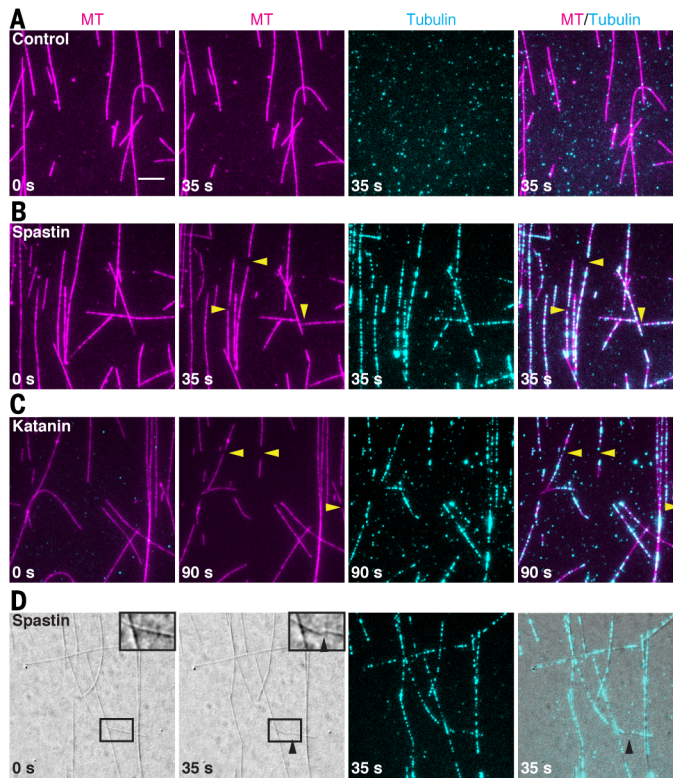
ected by soluble GTP-tubulin incorporation. Frequent nanoscale damage events were visible when severing events were extremely sparse: As early as 35 s, the density of spastin-induced nanoscale damage sites was  $0.35 \pm 0.01 \mu\text{m}^{-1}$ , compared with  $0.0008 \pm 0.0004 \mu\text{m}^{-1}$  for severing events (fig. S3, A and D). Thus, most nanoscale damage events did not lead to macroscopic severing events. Once a sufficient number of tubulin dimers was removed from the lattice, the microtubule unraveled and a macroscopic severing event was visible. Consistent with this, we observed an abrupt increase in mesoscale severing at 120 and 90 s for spastin and katanin, respectively (figs. S3D and S4D).

Next, we probed the effect of soluble tubulin on spastin microtubule severing by performing severing assays in the presence of fluorescently

## Fig. 2. Spastin- and katanin-catalyzed nanoscale damage is repaired by spontaneous tubulin incorporation.

(A and B) HiLyte 647-labeled GMPCPP-microtubules (MT) incubated with buffer (A) or 10 nM spastin (B) for 35 s and then incubated with 1  $\mu$ M HiLyte 488-labeled GTP-tubulin and washed to remove excess tubulin (Materials and methods). Arrowheads indicate severing events. Scale bar, 5  $\mu$ m. (C) HiLyte 647-labeled GMPCPP-microtubules incubated with 2 nM katanin for 90 s and then incubated with 1  $\mu$ M HiLyte 488-labeled GTP-tubulin and washed to remove excess tubulin

(Materials and methods). Arrowheads indicate severing events. (D) DIC-imaged unlabeled GMPCPP-microtubules incubated with 10 nM spastin and then with 1  $\mu$ M HiLyte 488-labeled GTP-tubulin (cyan) and washed to remove excess tubulin (Materials and methods). Insets correspond to boxed areas and show the progression to a severing event. Arrowheads indicate the severing site.



labeled soluble tubulin (fig. S5). This allowed us to detect microtubule nanoscale damage and severing simultaneously. Spastin-induced severing was not significantly affected with 100 nM tubulin, even though we observed incorporation of HiLyte 488-labeled tubulin into microtubules (Fig. 3A, fig. S5, and Materials and methods). However, severing was considerably reduced in the presence of 2  $\mu$ M soluble tubulin (Fig. 3A), and in this case, tubulin fluorescence intensity at repair sites was also significantly higher (Fig. 3B). Thus, the tubulin extraction activity of the enzyme was not significantly inhibited by soluble tubulin as proposed previously for katanin (35), but the rate of tubulin incorporation at nanoscale damage sites increased with tubulin concentration. This higher rate of tubulin incorporation at damage sites delays (and can even prevent) the completion of a severing event. Consistent with this, the time between the incorporation of HiLyte 488-tubulin at a nanoscale damage site and the completion of a severing event was longer in the presence of 2  $\mu$ M tubulin than in the presence of 100 nM tubulin (Fig. 3C). Thus, whereas almost all nanoscale damage sites detectable under our experimental conditions proceeded to complete severing within 65 s after tubulin incorporation in the presence of 100 nM soluble tubulin, only 47% did so at 2  $\mu$ M tubulin (Fig. 3D). We also monitored live the addition of single fluorescently labeled tubulin dimers by

TIRF microscopy (Fig. 3E and Materials and methods). Fluorescence intensity analyses revealed that repair proceeded mainly through the incorporation of tubulin heterodimers and not through the addition of larger tubulin polymers or aggregates because the fluorescence intensity distribution of incorporated tubulin was similar to that of single tubulin subunits immobilized to glass (Fig. 3F).

### Severing enzymes introduce GTP-tubulin islands

To rule out repair as an artifact of working with stabilized microtubules (either Taxol or GMPCPP stabilized), we extended our experiments to non-stabilized GDP-microtubules. We polymerized GDP-microtubules from axonemes and stabilized their ends with a GMPCPP cap to avoid spontaneous depolymerization (Materials and methods). We then introduced spastin in the absence or presence of fluorescently labeled soluble GTP-tubulin. Within 50 s of introducing 5 nM spastin and 5  $\mu$ M soluble tubulin [tubulin concentrations *in vivo* are 5 to 20  $\mu$ M (36, 37)], we observed the incorporation of tubulin as puncta along microtubules (Fig. 3G and movie S1). At these enzyme and tubulin concentrations, most tubulin incorporation sites did not progress to a severing event, and the severing rate was considerably lower than in the absence of soluble tubulin (Fig. 3H). However, tubulin incorpora-

tion always preceded microtubule severing. No repair sites were observed in the absence of spastin. Thus, the local balance between active tubulin removal catalyzed by the enzyme and passive tubulin incorporation determines whether a nanoscale damage site progresses to a mesoscale severing event or fails to do so because of the repair with GTP-tubulin from the soluble pool.

We also visualized the lattice-incorporated tubulin at a higher resolution by using TEM. We generated recombinant human  $\alpha$ 1 $\beta$ III tubulin with an engineered FLAG tag at the  $\beta$ -tubulin C terminus (38). We then used this recombinant tubulin to repair brain microtubules damaged at the nanoscale by spastin. The presence of the FLAG tag on the recombinant tubulin allowed specific detection of recombinant tubulin both in fluorescence and TEM images with the use of fluorescent or gold-conjugated secondary antibodies against FLAG antibodies (Materials and methods). Fluorescence microscopy revealed that the recombinant tubulin robustly incorporates along microtubules with nanoscale damage by spastin with ATP. No incorporation was detected with spastin and adenosine 5'-O-(3-thiotriphosphate) (ATP- $\gamma$ -S) (fig. S6). TEM showed the discrete, productive incorporation of recombinant  $\alpha$ 1 $\beta$ III tubulin in islands along microtubules and the absence of tubulin aggregates at nanoscale damage sites (fig. S7). The FLAG primary and secondary gold-conjugated antibodies are specific for the recombinant tubulin, as brain microtubules showed only background antibody decoration (fig. S7, C and D). In the absence of recombinant soluble tubulin in the reaction, microtubules were robustly damaged at the nanoscale under these conditions (fig. S7E). Moreover, neither recombinant tubulin incorporation nor association with the microtubule lattice was observed by fluorescence and TEM assays with the slow-hydrolyzing analog ATP- $\gamma$ -S (figs. S6 and S7, A and C). Thus, soluble tubulin was incorporated productively into the microtubule lattice at nanoscale damage sites created by spastin in an ATP hydrolysis-dependent manner.

### Severing enzymes promote rescues

Because spastin and katanin catalyze GTP-tubulin incorporation along microtubules, we next examined their effects on microtubule dynamics. It has been recognized for 30 years that tubulin incorporation into a growing microtubule stimulates hydrolysis of the bound GTP. The resulting GDP-tubulin lattice is unstable but is protected from depolymerization by a layer of GTP-tubulin. This GTP cap at the microtubule end results from a lag between the GTP hydrolysis rate on the incorporated tubulin and the microtubule growth speed (30, 31, 39–42). More recently, islands of GTP-tubulin were detected along microtubules in cells and were correlated with rescue (34, 43)—the transition from depolymerization to growth, one of the parameters of microtubule dynamic instability. As in stabilized GMPCPP-microtubules and GMPCPP-capped GDP-microtubules, the newly perfused GTP-tubulin was

rapidly incorporated along the GDP-microtubule lattice of dynamic microtubules in the presence of spastin and katanin with ATP; by contrast, in the control without ATP, addition was visible only at microtubule ends (Fig. 4, A to D, and movies S2 and S3). We then characterized microtubule dynamics in the presence of spastin or katanin at physiological concentrations [25 nM; spastin and katanin concentrations in HeLa cells are 46 and 28 nM, respectively (37)]. At these enzyme concentrations, we observed robust microtubule severing and internal GTP-tubulin incorporation. Spastin and katanin increased rescue frequencies by factors of ~13- and 9, respectively (with  $0.5 \pm 0.2 \text{ min}^{-1}$  for the control versus  $6.6 \pm 1.6 \text{ min}^{-1}$  and  $4.5 \pm 0.7 \text{ min}^{-1}$  for spastin and katanin, respectively) (Fig. 4E). Whereas only 13%

of the depolymerization events were rescued in the control, 61% were rescued in the presence of spastin or katanin (Fig. 4F). Consistent with their promotion of tubulin exchange along the microtubule shaft, spastin and katanin had no significant effect on rates of microtubule growth and catastrophe (Fig. 4, G and H). This is in contrast to other rescue-promoting factors, such as cytoplasmic linker-associated proteins, which promote rescue by increasing the on rate of tubulin dimers at microtubule ends and thus decrease catastrophe and increase growth rates (44), or conventional microtubule-associated proteins (MAPs) such as MAP2, which promote rescue by stabilizing the microtubule lattice (45).

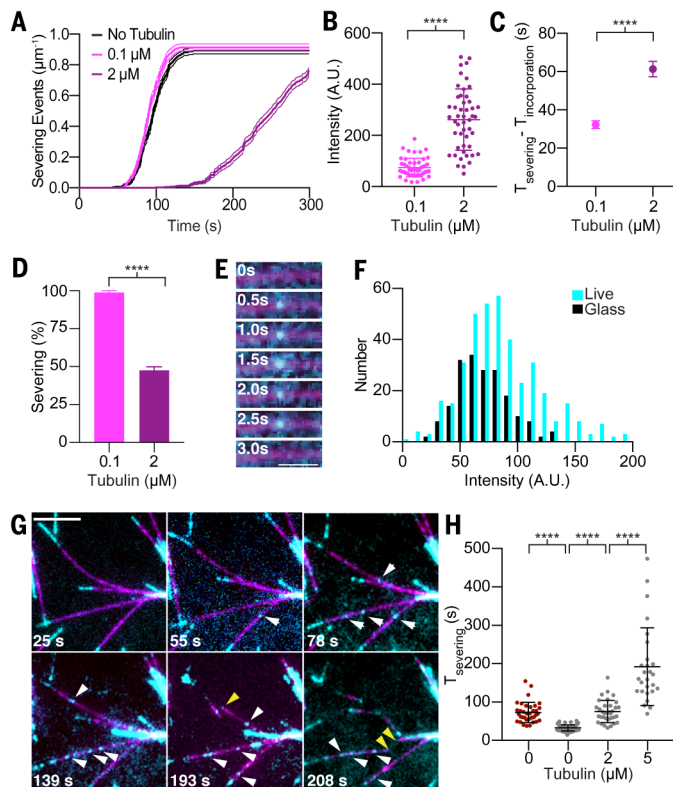
In our dynamics assays, tubulin was continually extracted by the enzyme, while at the same

time the lattice was healed with newly incorporated GTP-tubulin that was gradually converted into GDP-tubulin. To decouple these processes and establish directly whether the GTP-tubulin islands introduced by these enzymes can act as microtubule rescue sites, we introduced non-hydrolyzable GTP-tubulin islands into the microtubule. We induced nanoscale damage to a GMPCPP-capped GDP-microtubule with spastin or katanin and healed it with GMPCPP-tubulin, removed the enzyme and GMPCPP-tubulin from the chamber; and initiated microtubule depolymerization through laser ablation close to the GMPCPP cap (Fig. 5; fig. S8, A to C; and Materials and methods). No GMPCPP-tubulin incorporation was detected in the control performed in the presence of enzyme without ATP. These microtubules depolymerized all the way to the seed upon ablation (Fig. 5B and fig. S8A). In contrast, microtubules with GMPCPP-tubulin islands incorporated along their lengths through the ATP hydrolysis-dependent activity of spastin or katanin were stabilized against depolymerization at the location of the island (Fig. 5C and fig. S8B), despite the absence of soluble tubulin in the chamber: 75% and 76% paused when they encountered a GMPCPP island introduced by spastin and katanin, respectively (Fig. 5D; fig. S8, A to C; and movie S4). Those that depolymerized through the island showed a decrease in the depolymerization speed (Fig. 5E and fig. S8D). Moreover, fluorescence intensity analysis revealed that GMPCPP islands that paused depolymerization were statistically significantly brighter than those that did not (Fig. 5F and fig. S8E). Next, we wanted to establish whether these enzyme-generated GMPCPP islands were competent to support microtubule regrowth. We again performed the above-described experiment, but during the last step we introduced 7  $\mu\text{M}$  soluble GTP-tubulin into the chamber (Fig. 5, A, G, and H, and movie S5). Whereas at these tubulin concentrations rescue events were very rare in the control, we saw a higher probability of rescue of microtubules with spastin-incorporated GMPCPP islands (Fig. 5I). When the GMPCPP island did not support a rescue, it did slow down depolymerization (Fig. 5J). Moreover, fluorescence intensity analysis revealed that GMPCPP islands that supported rescues were significantly brighter than those that did not (Fig. 5K). Thus, microtubule dynamics measurements and experiments with GMPCPP-tubulin islands indicate that GTP islands introduced in a microtubule severing enzyme-dependent manner promote microtubule rescue and that there is a minimal local GTP-tubulin density required to robustly support rescue at that site. Because the microtubule is rescued when the balance shifts from net tubulin loss to net tubulin addition, it is likely that the correlation between the size of the GTP-tubulin island and rescue probability will vary with the tubulin concentration or the presence of MAPs. Thus, smaller GTP-tubulin islands may still be effective as rescue sites at higher tubulin concentrations or in the presence of MAPs that increase the tubulin on rate.

### Fig. 3. Incorporation of soluble tubulin into spastin-induced nanoscale damage sites inhibits microtubule severing.

(A) Severing rates in the presence of soluble tubulin ( $n = 31$ , 28, and 36 microtubules from multiple chambers for no tubulin, 100 nM tubulin, and 2  $\mu\text{M}$  tubulin, respectively). Thin lines indicate SEM.

(B) Intensity distribution of fluorescent tubulin puncta incorporated at spastin-induced nanoscale damage sites ( $n = 50$  and 49 puncta from multiple chambers for 100 nM and 2  $\mu\text{M}$  tubulin, respectively). Bars indicate the means and SD. A.U., arbitrary units. (C) Repair at damage sites delays severing ( $n = 81$  and 83 severing events from multiple chambers for 100 nM and 2  $\mu\text{M}$  tubulin, respectively).  $T_{\text{severing}}$  and  $T_{\text{incorporation}}$ , time required for a severing event and for initial incorporation of tubulin, respectively. (D) Fraction of GMPCPP-microtubules severed by 20 nM spastin within 65 s of initial tubulin incorporation in the presence of 100 nM and 2  $\mu\text{M}$  HiLyte 488-labeled soluble tubulin. Error bars indicate SEM in (C) and (D). (E) Live imaging of Alexa 488-labeled GTP-tubulin (cyan) incorporation into HiLyte 647-labeled GMPCPP-microtubules (magenta) after spastin-induced damage. Scale bar, 1.5  $\mu\text{m}$ . (F) Fluorescence intensity distribution of Alexa 488-labeled tubulin (labeling ratio, ~1.0) immobilized on glass or incorporated into spastin-induced nanoscale damage sites ( $n = 188$  and 398 for glass-immobilized and microtubule-incorporated particles, respectively). (G) Spastin-induced nanoscale damage and spontaneous tubulin repair of GDP-microtubules (magenta) grown from axonemes and stabilized with a GMPCPP cap (bright cyan) in the presence of spastin (5 nM) and 5  $\mu\text{M}$  soluble HiLyte 488-labeled GTP-tubulin (cyan). Images were bleach corrected. White arrowheads, tubulin incorporation sites; yellow arrowheads, severing events. Scale bar, 5  $\mu\text{m}$ . (H) Average completion time of a severing event after spastin perfusion. Brown, GMPCPP-microtubules; gray, GMPCPP-capped GDP-microtubules in the absence or presence of soluble tubulin ( $n = 36$ , 63, 34, and 27 microtubules from multiple chambers for GMPCPP-microtubules and GMPCPP-capped GDP-microtubules with 0, 2  $\mu\text{M}$ , and 5  $\mu\text{M}$  soluble GTP-tubulin, respectively). Bars indicate the means and SD. \*\*\*\* $P < 0.0001$ , determined by a two-tailed  $t$  test, for (B), (C), (D), and (H).



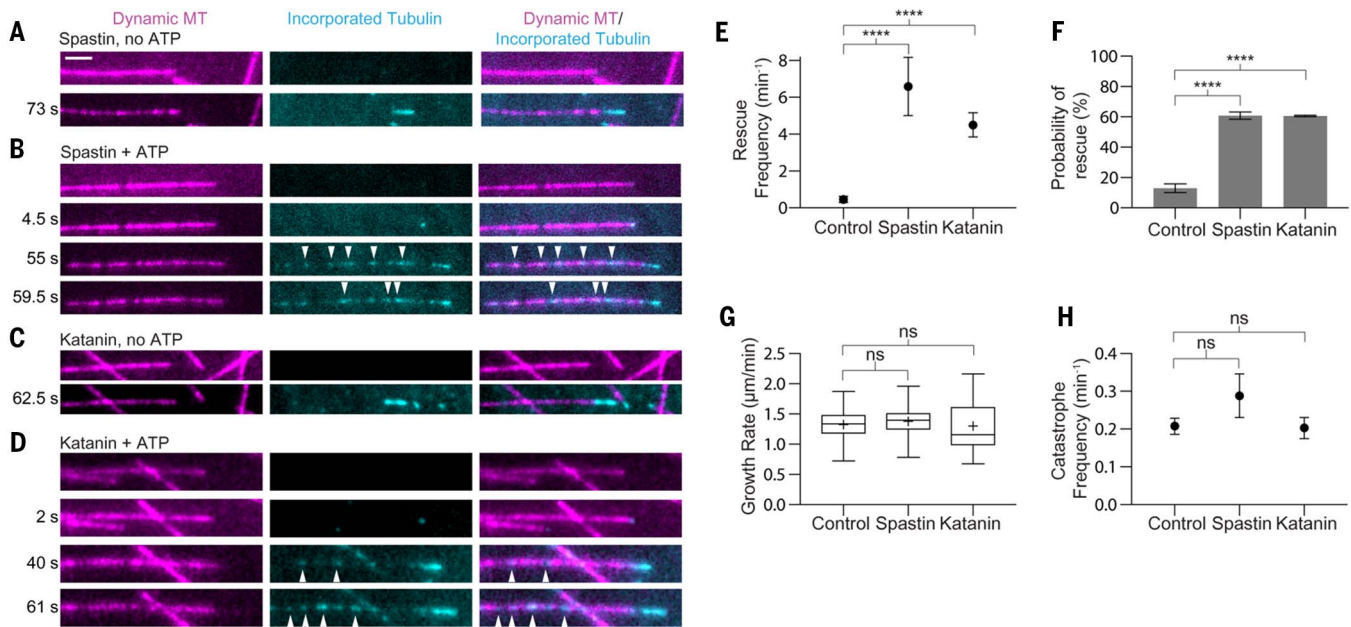


**Fig. 4. Spastin and katanin promote GTP-tubulin island formation and increase rescues.** (A and B) Time course of a dynamic 10% HiLyte 647-labeled microtubule at 12  $\mu\text{M}$  tubulin in the presence of 25 nM spastin without (A) or with (B) ATP showing HiLyte 488-labeled tubulin incorporation at the microtubule tip (A) or incorporation (arrowheads) along the microtubule in addition to the tip (B). The first micrograph for each condition was recorded just before the perfusion of the chamber with 12  $\mu\text{M}$  10% HiLyte 488-labeled tubulin. Scale bar, 2  $\mu\text{m}$ . (C and D) Time course of a dynamic 10% HiLyte 647-labeled microtubule at 12  $\mu\text{M}$  tubulin in the presence of 25 nM katanin without (C) or with (D) ATP showing HiLyte 488-labeled tubulin incorporation at the microtubule tip (C) or incorporation (arrowheads) along the microtubule in addition to the tip (D). The first micrograph for each condition was recorded just before the perfusion of the chamber with 12  $\mu\text{M}$  10% HiLyte

488-labeled tubulin. (E) Rescue frequency at 10  $\mu\text{M}$  tubulin in the absence or presence of 25 nM spastin and 25 nM katanin with ATP ( $n = 47, 45,$  and  $61$  microtubules from multiple chambers for the control without enzyme, spastin, and katanin, respectively).  $****P < 0.0001$ , determined by the Mann-Whitney test. (F) Probability of rescue of a depolymerizing microtubule in the absence or presence of spastin and katanin with ATP ( $n = 68, 57,$  and  $78$  depolymerization events for the control, spastin, and katanin, respectively).  $****P < 0.0001$ , determined by a two-tailed  $t$  test. (G and H) Growth rates (G) and catastrophe frequency (H) in the absence or presence of spastin and katanin with ATP [ $n = 56, 37,$  and  $34$  growth events for the control, spastin, and katanin, respectively, in (G) and  $n = 62, 70,$  and  $71$  microtubules for the control, spastin, and katanin, respectively, in (H)]. Plus signs in (G) indicate the means. ns, not significant. Error bars indicate SEM throughout.

### Severing enzyme-generated GTP islands recruit EB1

The GTP state of tubulin is recognized by MAPs belonging to the end-binding (EB) protein family. EB1 preferentially binds to growing microtubule ends by sensing the GTP [or GDP-inorganic phosphate ( $P_i$ )] state of tubulin (46, 47). Consistent with the creation of GTP-tubulin islands, in the presence of spastin or katanin and ATP we observed EB1 not only at the growing ends as in the control but also as distinct puncta along microtubules (Fig. 6, A to D). These puncta are reminiscent of the EB3 puncta observed at sites of tubulin repair after laser-induced damage (34). Of the newly incorporated GTP-tubulin islands, 89% colocalized with EB1 (Fig. 6, E and F). These EB1 puncta were transient, consistent with the dynamic removal and incorporation of new tubulin into the lattice and the gradual GTP hydrolysis of the incorporated tubulin (Fig. 6, A and C; fig. S9; and movie S6). Consistent with a protective effect of the GTP islands, microtubule dynamics assays in the presence of spastin and EB1 revealed that 74% of rescues were associated with the presence of EB1 at the rescue site (fig. S10A). This number is significantly higher than the pre-

diction given by the random superposition of EB1 puncta and rescue events (74% versus 14%;  $P < 0.0001$  by Fisher's exact test) (Materials and methods). Similarly, 63% of rescues in the presence of katanin occurred at the site of an EB1 spot (fig. S10B), compared with 0% when the distribution was randomized ( $P < 0.00001$  by Fisher's exact test) (Materials and methods). Laser ablation of microtubules peppered with EB1 puncta also revealed a marked increase in rescue frequency. Whereas microtubules were rescued from 100% of ablation-induced depolymerization events within 4 s, they were rescued from only 15% of events in the presence of spastin and ATP- $\gamma$ -S (Fig. 6, G and H). Similar results were obtained with katanin (Fig. 6I and movie S7). Thus, the ATP-dependent action of the enzyme that promotes tubulin exchange within the lattice is required for the observed increase in rescue frequency.

### Severing amplifies microtubule mass and number

The GDP-tubulin lattice is unstable and, when exposed by laser ablation, is rapidly depolymerized at the plus ends, even in the presence of soluble tubulin (Fig. 7A), a result consistent

with those of classic experiments performed with laser-ablated or mechanically cut microtubules (28, 29, 48–51). Surprisingly, at 12  $\mu\text{M}$  tubulin, the majority of new plus ends generated by spastin or katanin were stable and rapidly reinitiated growth (Fig. 7, B and C). By contrast, in the absence of either enzyme or in the presence of spastin or katanin and ATP- $\gamma$ -S, new plus ends generated through laser ablation rapidly depolymerized (Figs. 6, H and I, and 7A). This indicates that it is not the passive binding of the protein that stabilizes the new plus ends against spontaneous depolymerization but the ATP-dependent incorporation of GTP-tubulin at severing sites. The minus ends were stable regardless of whether they were generated through enzyme action or laser ablation, consistent with results of earlier experiments using laser ablation (28, 29). Thus, when local tubulin extraction by spastin or katanin outpaces the rate of tubulin incorporation, a severing event occurs and the newly severed microtubule ends emerge with a high density of GTP-tubulin that is protective (Fig. 7, B and C). Moreover, the plus ends that depolymerize immediately after severing resume growth after a lower net loss of polymer mass (fig. S8, F and G).

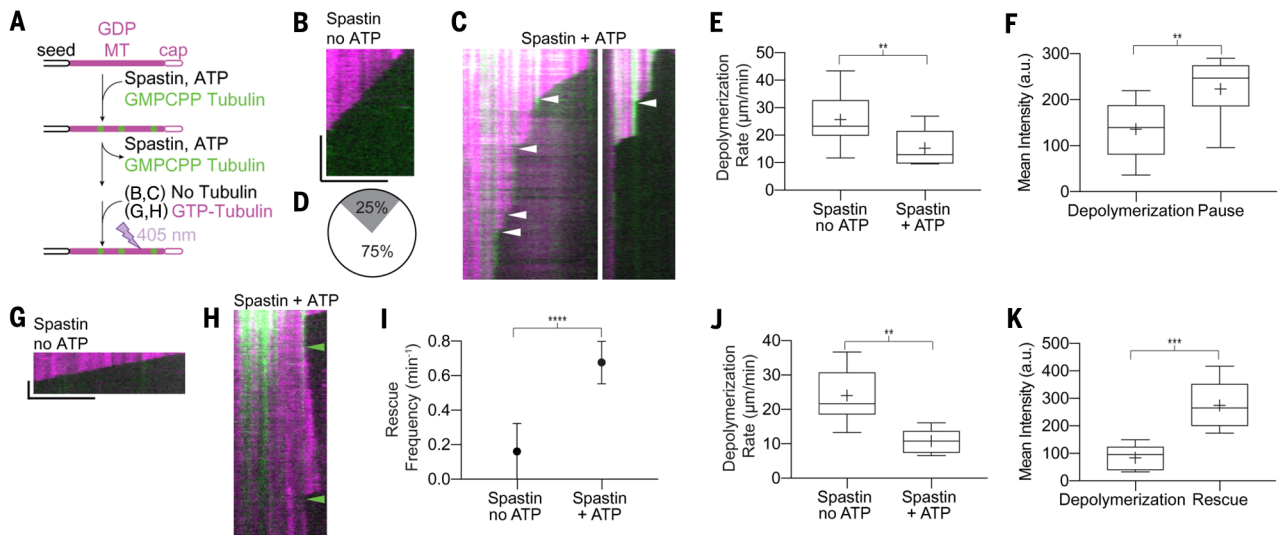


**Fig. 5. Enzyme-generated GMPCPP islands protect against depolymerization and act as rescue sites.** (A) Experiment schematic. GDP-microtubules (solid magenta) were polymerized from seeds and capped with GMPCPP-tubulin (magenta outline). Spastin, ATP, and GMPCPP-tubulin (green) were added and washed out of the chamber. Microtubules were laser ablated in the absence (B to F) or presence (G to K) of GTP-tubulin (Materials and methods). (B) Kymograph of a depolymerizing laser-ablated microtubule (magenta) preincubated with spastin and no ATP. Horizontal scale bar, 5  $\mu\text{m}$ ; vertical bar, 10 s. (C) Kymographs of depolymerizing laser-ablated microtubules pausing at GMPCPP-tubulin islands (green) introduced by spastin with 1 mM ATP. Arrowheads, pauses. (D) Pie chart showing the proportion of depolymerization events that paused at GMPCPP islands (white) or did not (gray) ( $n = 44$  events). (E) Depolymerization rates of microtubules without GMPCPP islands preincubated with spastin and no ATP or of microtubules depolymerized through GMPCPP islands introduced by spastin with 1 mM ATP ( $n = 17$  and 7 microtubules for no ATP and ATP,

respectively). (F) Fluorescence intensity of GMPCPP islands through which microtubules depolymerized or paused ( $n = 9$  and 14 islands, respectively). (G and H) Kymographs of laser-ablated microtubules in the presence of 7  $\mu\text{M}$  soluble GTP-tubulin after preincubation with spastin and no ATP showing complete depolymerization (G) or rescue (arrowheads) at a GMPCPP island introduced by spastin with ATP (H). Horizontal scale bar, 5  $\mu\text{m}$ ; vertical bar, 20 s. (I) Rescue frequency for laser-ablated microtubules incubated with or without ATP ( $n = 23$  and 24 microtubules with and without ATP, respectively). (J) Depolymerization rates in the presence of 7  $\mu\text{M}$  GTP-tubulin for microtubules preincubated with spastin and no ATP or for microtubules that depolymerized through GMPCPP islands introduced by spastin with ATP ( $n = 9$  and 6 microtubules without and with ATP, respectively). (K) Fluorescence intensity of GMPCPP islands that did not stop depolymerization ( $n = 6$ ) or at which microtubules were rescued in the presence of spastin and ATP ( $n = 9$ ).  $**P < 0.01$ ,  $***P < 0.001$ , determined by the Mann-Whitney test. Plus signs in (E), (F), (J), and (K) indicate means. Error bars indicate SEM throughout.

Thus, the increase in microtubule number with each severing event (Fig. 7, D and E) synergizes with the higher rescue frequency to produce a rapid amplification of total microtubule number and mass (Fig. 7, F to J).

## Discussion

The classical view of microtubule dynamics has been that tubulin dimer exchange occurs exclusively at microtubule ends through polymerization and depolymerization (30, 52). By visualizing a severing reaction at the ultrastructural level, we have shown that spastin and katanin extract tubulin subunits from the microtubule (Fig. 1) and that this ATP hydrolysis-dependent tubulin removal is counteracted by spontaneous lattice incorporation of soluble GTP-tubulin (Figs. 2 to 4 and figs. S5 to S7). The nanoscale-damaged microtubules do not immediately unravel but are long-lived enough to have a chance to heal through the productive incorporation of tubulin into the lattice. Because longitudinal lattice contacts are stronger than lateral ones (42), we speculate that tubulin dimer loss from the microtubule wall has a slight longitudinal bias that proceeds along the protofilament. This would give the microtubule a chance to heal before it is severed across and

generate GTP-tubulin islands that consist of several tubulin dimers in the longitudinal direction. The geometry of the nanoscale damage sites and the mechanism of tubulin incorporation and conformational changes at these sites will be exciting and fundamental areas for future exploration.

This mechanism of lattice repair can explain the earlier observation of the inhibition of katanin severing by soluble tubulin (53, 54). The ragged, Swiss cheese nature of the nanoscale-damaged microtubules is conducive to healing, as the incoming tubulin dimers can make stabilizing lateral interactions. Thus, depending on the local rates of the severing enzyme-catalyzed tubulin removal and the spontaneous incorporation of new GTP-tubulin into the lattice, the action of a microtubule-severing enzyme results in a severing event where the newly emerging ends have a high density of GTP-tubulin or a microtubule that preserves integrity but acquires a GTP island at the site of enzyme action. The higher GTP density at the newly severed ends can also act to quickly recruit molecular motors and MAPs that can modulate the fate of the newly generated end.

Although in vitro microtubule repair after the introduction of defects through laser-induced photodamage (34) or mechanical stress (33, 55)

has been reported previously, our study identifies a family of enzymes as biological agents that promote the ATP-dependent incorporation of GTP-tubulin islands into microtubules. Microtubule repair has a high incidence in vivo at microtubule crossovers or bundles (34), where microtubule-severing enzymes have been shown to act (7, 8, 17, 56). Our findings thus suggest that the high incidence of repair at these sites is due not exclusively to mechanical damage (34) but also to the action of microtubule-severing enzymes. As spastin and katanin preferentially target glutamylated microtubules (13, 57, 58), they may also selectively rejuvenate aging microtubules with accumulated glutamylation marks through GTP-tubulin incorporation. GTP-tubulin islands have been identified along axonal microtubules (59), a neuronal compartment where severing enzymes act. This finding raises the possibility that severing enzymes are also used as quality control and maintenance factors in hyperstable microtubule arrays, such as those in axons, centrioles, and cilia, where spastin and katanin are important for biogenesis and maintenance (2, 5, 13, 14) and where spastin and katanin may serve to remove and replace old, possibly damaged tubulin subunits without affecting overall microtubule

organization. Future work should establish how impaired lattice repair contributes to the disease phenotypes seen in patients with spastin and katanin mutations.

Our study shows that the severing enzyme-catalyzed incorporation of GTP-tubulin along microtubules has two physiological consequences: It increases the frequency at which microtubules are rescued (Figs. 4 to 6), and it stabilizes newly severed plus ends that emerge against de-

polymerization with a high density of GTP-tubulin (Fig. 7). Thus, microtubule dynamics can be modulated not only by factors that affect tubulin incorporation at microtubule ends but also by severing enzymes that promote the exchange of tubulin subunits within the microtubule shaft. The synergy between the increased rescue rates and the stabilization of the newly severed ends leads to microtubule amplification in the absence of a nucleating factor, explaining why, paradox-

ically, the loss of spastin and katanin results in the loss of microtubule mass in many systems (2, 23, 25, 27). Such a mechanism of polymer amplification has parallels to the actin cytoskeleton, where severed filaments are used for templated actin polymerization [(26, 60); reviewed in (61)]. When severing enzymes are expressed at high levels or are positively regulated, tubulin extraction outpaces repair and the microtubule array disassembles. Cells likely modulate severing activity and the rate of tubulin lattice incorporation through the action of MAPs to elicit these two different outcomes. This regulation will be a notable area of future exploration.

## Materials and methods

### Protein expression and purification

*Drosophila melanogaster* full-length spastin was purified by affinity chromatography and ion exchange as previously described (62). *Caenorhabditis elegans* MBP-tagged katanin Meil/Mei2 (12) was purified on amylose resin. The affinity tag was removed by tobacco etch virus protease, and the protein was further purified on an ion exchange MonoS column (GE Healthcare) as previously described (63). Peak fractions were concentrated, buffer was exchanged into 20 mM HEPES (pH 7.0), 300 mM KCl, 10 mM MgCl<sub>2</sub>, and 1 mM TCEP, and fractions were flash frozen in small aliquots in liquid nitrogen. *Homo sapiens* EB1-green fluorescent protein (GFP) was expressed and purified as previously described (64). Human  $\alpha$ 1A $\beta$ III tubulin with an engineered FLAG tag at the  $\beta$ -tubulin C terminus was expressed by using baculovirus and purified as described previously (38).

### Transmission electron microscopy of microtubule-severing reactions

Taxol-stabilized GDP-microtubules were prepared by polymerizing 10  $\mu$ l of 100  $\mu$ M glycerol-free porcine tubulin (Cytoskeleton, Denver, CO) in 80 mM K-PIPES (pH 6.8), 1 mM MgCl<sub>2</sub>, 1 mM EGTA, 10% DMSO, and 1 mM GTP for 1 hour in a 37°C water bath. Taxol was added to 20  $\mu$ M final concentration, and the reaction was incubated on the bench top for 1 to 2 hours. Microtubules were loaded onto a 60% glycerol cushion [BRB80, 60% (v/v) glycerol, and 20  $\mu$ M Taxol] at 37°C by using a pipette tip with the tip cut off. Non-polymerized tubulin was removed by centrifugation in a TLA100 rotor at 35,000 rpm for 15 min at 37°C. The pellet was gently resuspended to 2.5  $\mu$ M tubulin in BRB80 supplemented with 20  $\mu$ M Taxol and 1 mM GTP at 37°C by using a pipette tip with the tip cut off.

For GDP-microtubules, all polymerization and severing reactions were performed at 37°C. Twenty microliters of 100  $\mu$ M glycerol-free porcine tubulin (Cytoskeleton) was polymerized in 10% DMSO, 1 mM GTP, and 10 mM MgCl<sub>2</sub> for 1 hour at 37°C in a water bath. The microtubules were passed through a 60% glycerol cushion [BRB80, 60% (v/v) glycerol, and 1 mM GTP] by using a TLA100 rotor at 53,000  $\times$  g for 15 min to remove nonpolymerized tubulin. The pellet was washed twice using 50  $\mu$ l of buffer (BRB80, 10% DMSO, 1 mM GTP)

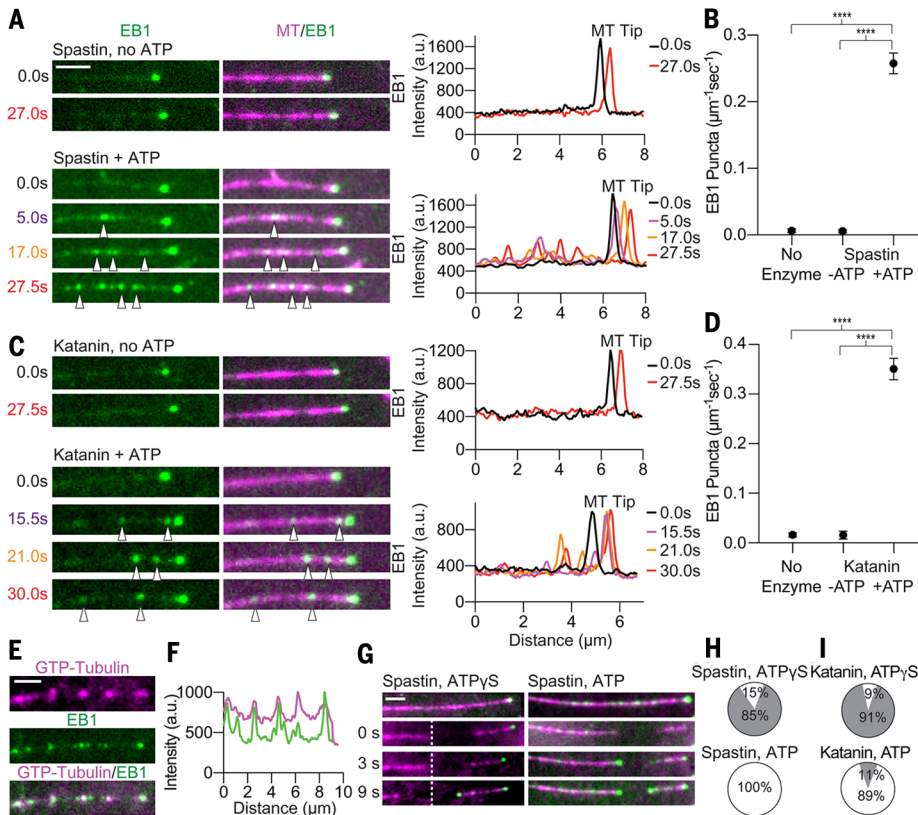


**Fig. 6. Spastin- and katanin-generated GTP-tubulin islands recruit EB1.** (A) Time course of EB1-GFP on a dynamic microtubule in the presence of 25 nM spastin without or with ATP. Scale bar, 2  $\mu$ m. Line scans on the right show EB1-GFP intensity profiles along the microtubule at the indicated times. Intensity profiles start on the microtubule lattice and end at the microtubule tip. Arrowheads show lattice EB1 puncta. (B) Density of EB1-GFP puncta on microtubules incubated without spastin or with spastin without and with ATP. Error bars indicate SEM. \*\*\*\* $P < 0.0001$ . (C) Time course of EB1-GFP on a dynamic microtubule in the presence of 25 nM katanin without and with ATP. Intensity profiles are as in (A). Arrowheads show lattice EB1 puncta. (D) Density of EB1-GFP puncta on microtubules incubated without katanin or with katanin without or with ATP. Error bars indicate SEM. \*\*\*\* $P < 0.0001$ . (E) Colocalization of newly incorporated GTP-tubulin (top) and EB1-GFP (middle) in the presence of spastin and ATP. (Bottom) Overlay. Images were acquired immediately after the perfusion of the chamber with enzyme and EB1-GFP. Scale bar, 2  $\mu$ m. (F) Fluorescence intensity of incorporated tubulin (magenta) and EB1-GFP (green) along the microtubule lattice in (E) showing their colocalization. Eighty-nine percent of tubulin islands colocalize with EB1-GFP ( $n = 38$  puncta from 22 microtubules from multiple chambers measured immediately after perfusion with 10% HyLite 647-tubulin). (G) Time course of laser-ablated dynamic microtubules (magenta) incubated with 25 nM spastin with ATP- $\gamma$ -S or spastin with ATP in the presence of 50 nM EB1-GFP (green) (Materials and methods). The dotted line marks the ablated region and the start of depolymerization. Scale bar, 2  $\mu$ m. (H and I) Pie charts show the fates of plus ends generated through laser ablation of microtubules incubated with spastin (H) or katanin (I) with ATP- $\gamma$ -S or ATP. The percentage of plus ends that depolymerized (gray) or were rescued (white) within 4 s after ablation is shown ( $n = 13$  and 13 microtubules from multiple chambers for spastin with ATP- $\gamma$ -S and ATP, respectively;  $n = 54$  and 9 microtubules from multiple chambers for katanin with ATP- $\gamma$ -S and ATP, respectively).

### Fig. 7. Severing enzyme-based microtubule number and mass amplification.

(A) Plus ends generated through laser ablation depolymerize. The pie chart shows the percentages of plus ends that are stable (white) or depolymerize (gray) ( $n = 32$  microtubules from multiple chambers). Scale bar, 5  $\mu\text{m}$ . The dashed line marks the ablated region and the start of depolymerization.

(B and C) Spastin (B)- or katanin (C)-severed ends emerge with newly incorporated GTP-tubulin and are stable. The pie charts show the percentages of plus ends that are stable (white) or depolymerize (gray) ( $n = 96$  and 94 microtubules from multiple chambers for spastin and katanin, respectively). White and yellow arrowheads indicate tubulin incorporation and a severing event, respectively.

(D and E) Time-lapse images showing consecutive spastin (D)- or katanin (E)-induced severing events on a microtubule. Lines and numbers indicate individual microtubules after severing. + and - mark microtubule ends. Magenta, microtubule; green, incorporated tubulin. Scale bars, 2  $\mu\text{m}$ .

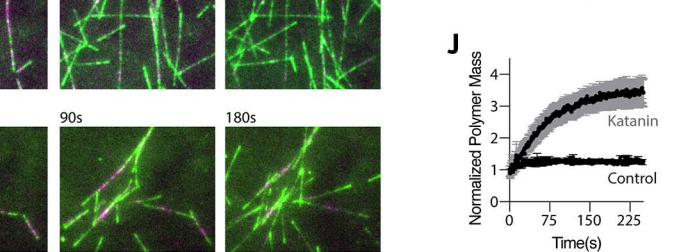
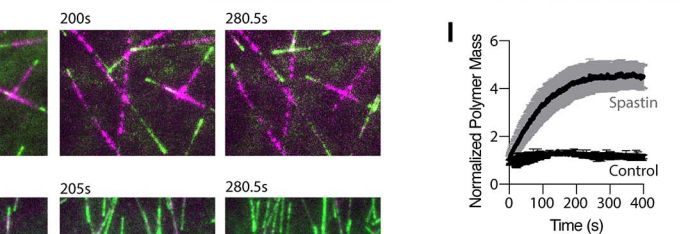
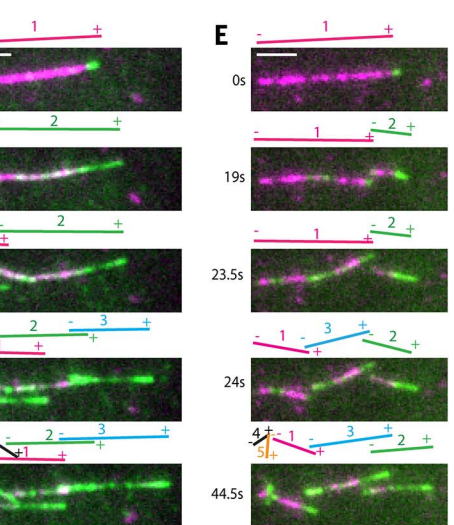
(F) Time-lapse images showing microtubule dynamics at 12  $\mu\text{M}$  tubulin in the absence of a severing enzyme. Green, newly incorporated tubulin at the growing ends. The last two frames are bleach corrected. Scale bar, 5  $\mu\text{m}$ .

and gently resuspended to 30  $\mu\text{M}$  in the same buffer by using a pipette tip with the tip cut off.

GMPCPP-microtubules were prepared by polymerizing 20  $\mu\text{l}$  of 100  $\mu\text{M}$  glycerol-free porcine tubulin (Cytoskeleton) in 1 mM GMPCPP in BRB80 [80 mM PIPES-KOH (pH 6.8), 1 mM  $\text{MgCl}_2$ , 1 mM EGTA, 1 mM DTT] on ice for 5 min and then in a water bath at 37°C for 1 hour. Nonpolymerized tubulin was removed by centrifugation in a TLA100 rotor at 126,000  $\times g$  for 5 min at 37°C. The pellet was washed twice with 50  $\mu\text{l}$  of BRB80 at 37°C and resuspended in 50  $\mu\text{l}$  of ice-cold BRB80. The reaction mixture was kept on ice for 30 min and periodically mixed up and down to fully depolymerize microtubules. GMPCPP was added to 1 mM, and the polymerization reaction mixture was kept on ice for 10 min and then transferred to 37°C for 2 to 4 hours or overnight. Nonpolymerized tubulin was removed by centrifugation and washed as described above. The microtubule pellet was gently resuspended to 2.5  $\mu\text{M}$  tubulin in BRB80 by using a pipette tip with the tip cut off.

We found that performing severing reactions in the tube followed by pipetting onto EM grids resulted in microtubule breakage. We therefore first carried out severing reactions on the EM grid. Briefly, 2  $\mu\text{l}$  of microtubule solution (at 1 to 3  $\mu\text{M}$ ) in BRB80 [80 mM PIPES (pH 6.8), 1 mM  $\text{MgCl}_2$ , 1 mM EGTA] was applied to a glow-discharged Cu grid, followed by pipetting of 2  $\mu\text{l}$  of ATP solution (10 mM ATP in BRB80 supplemented with 20 mM Taxol for Taxol-stabilized microtubules) and 2  $\mu\text{l}$  of spastin (at 100 nM). The reaction was allowed to proceed on the grid for 1 min or as specified, after which the liquid was wicked off with calcium-free filter paper and the grid was stained with 0.75% (w/v) uranyl formate

and air-dried. Images were collected on a FEI Morgagni 286 electron microscope operated at 80 kV and equipped with an AMT lens-coupled 1k  $\times$  1k CCD camera. For the solution severing reaction time courses, 20  $\mu\text{l}$  of GMPCPP or Taxol-stabilized microtubules in BRB80 buffer at 2.5 and 1.0  $\mu\text{M}$  was applied to parafilm, followed by the addition of 20  $\mu\text{l}$  of 50 nM spastin or 200 nM katanin in 20 mM HEPES (pH 7.5), 300 mM KCl, 10 mM  $\text{MgCl}_2$ , 1 mM TCEP, and 1 mM ATP to a final concentration of 25 nM spastin and 100 nM katanin. For the solution severing reaction time courses of nonstabilized GDP-microtubules, 20  $\mu\text{l}$  of 30  $\mu\text{M}$  GDP-microtubules in the presence of 10% DMSO was incubated with 2  $\mu\text{l}$  of 20 nM katanin. Buffer without severing enzymes was added to microtubules as a negative control. The severing reaction mixtures were incubated for 30 s or 2 or 5 min, and carbon-coated grids (carbon film



ends. The last two frames are bleach corrected. Scale bar, 5  $\mu\text{m}$ . (G and H) Time-lapse images showing microtubule number and mass amplification through spastin (G) and katanin (H) severing. Green, newly incorporated HiLyte 488-tubulin perfused into the chambers together with the severing enzymes. (I and J) Microtubule mass as a function of time ( $n = 4, 5$ , and 4 chambers for the control, spastin, and katanin, respectively). Error bars indicate SEM.

only on 400 mesh; Ted Pella) were dipped into the reaction mixtures. Excess liquid was blotted with filter paper. Grids were washed three times with 40  $\mu$ l BRB80, stained with 0.75% (w/v) uranyl formate, and air-dried. Images were collected on a T12 Technai electron microscope (FEI) equipped with a 2k  $\times$  2k Gatan US1000 CCD camera. Images were collected at nominal magnifications of 550 $\times$ , 13,000 $\times$ , or 30,000 $\times$ , corresponding to pixel sizes of 84  $\text{\AA}/\text{pix}$ , 3.55  $\text{\AA}/\text{pix}$ , or 1.54  $\text{\AA}/\text{pix}$ , respectively.

#### **TIRF-based assays of tubulin incorporation into stabilized microtubules damaged by spastin and katanin**

Double-cycled, GMPCPP-stabilized microtubules (65) were polymerized from 2-mg/ml porcine brain tubulin (Cytoskeleton). The first polymerization was 1 hour, and the second polymerization step was at least 4 hours to obtain long microtubules. Then microtubules were centrifuged, resuspended in warm BRB80 [80 mM K-PIPES (pH 6.8), 1 mM  $\text{MgCl}_2$ , 1 mM EGTA], and stored at 37°C or room temperature (RT) before use. The same results were obtained regardless of whether the storage temperature was 37°C or RT. Taxol-stabilized microtubules (62) were polymerized from 5-mg/ml porcine brain tubulin containing 1% biotinylated and 20% HiLyte 647-labeled tubulin (Cytoskeleton) in BRB80 with 10% DMSO, 0.5 mM GTP, and 10 mM  $\text{MgCl}_2$ . After 1 hour of incubation at 37°C, 20  $\mu$ M Taxol was added and the mixture was further incubated overnight. Microtubules were then centrifuged through a 60% glycerol cushion for 12 min at 109,000  $\times$  g at 35°C. The microtubule pellet was washed with warm BRB80 supplemented with 14.3 mM 2-mercaptoethanol and 20  $\mu$ M Taxol and was resuspended gently in the same buffer.

Chambers for TIRF microscopy were assembled as previously described (62). Double-cycled GMPCPP-microtubules containing 1% biotinylated tubulin and 20% HiLyte 647-labeled tubulin (or unlabeled tubulin for the DIC assays) assembled as described above were immobilized in the chamber with 2-mg/ml NeutrAvidin (Thermo Fisher Scientific) and imaged by TIRF or DIC microscopy in severing buffer [BRB80 buffer with 2-mg/ml casein, 14.3 mM 2-mercaptoethanol, 2.5% glycerol, 50 mM KCl, 2.5 mM  $\text{MgCl}_2$ , 1 mM ATP, 1% Pluronic F127 (Life Technologies), and oxygen scavengers]. To introduce and detect nanoscale damage in microtubules (Fig. 2), immobilized microtubules were then incubated with 10 nM spastin or 2 nM katanin in severing buffer for 35 or 90 s, respectively. Microtubules in control experiments were incubated without severing enzyme. The enzyme mixture was then replaced with 1  $\mu$ M HiLyte 488-labeled tubulin (Cytoskeleton), 1 mM ADP, 0.5 mM GTP, 1% Pluronic F127, and 2.5-mg/ml casein in BRB80 and left to incubate for 5 min. The tubulin-containing solution was then washed out with 45  $\mu$ l of BRB80 supplemented with oxygen scavengers, 1.5-mg/ml casein, 10 mM 2-mercaptoethanol, and 1% Pluronic F127. Microtubules and HiLyte 488-labeled

tubulin were imaged by TIRF. Multiple fields of view were imaged. The same assay was performed for Taxol-stabilized microtubules, but in this case the repair step was performed with 0.1  $\mu$ M soluble tubulin to prevent microtubule nucleation in the presence of Taxol. For time-course experiments, the same protocol was used except that microtubules were incubated with 2 nM spastin (fig. S3) or 2 nM katanin (fig. S4) for 35 to 120 s. Control microtubules were incubated without severing enzyme for 120 s. HiLyte 488-labeled tubulin (1  $\mu$ M) was used for the repair step. For repair with 1  $\mu$ M recombinant human tubulin (fig. S6), nanoscale-damaged microtubules were incubated for 5 min with recombinant tubulin. Unincorporated tubulin was washed away, and tubulin incorporated into microtubules was detected by anti-FLAG M2 antibodies (Sigma-Aldrich; diluted 1:500) and goat anti-mouse antibodies conjugated with Alexa Fluor 488 (Invitrogen; diluted 1:1000). All assays were performed at RT. Details regarding image acquisition and analysis are described in the subsection below.

#### **Image acquisition and analysis of tubulin incorporation in GMPCPP- and Taxol-stabilized microtubules by TIRF microscopy**

Images were acquired by using a Nikon Ti-E microscope equipped with a 100 $\times$  1.49 NA oil objective and a TI-TIRF adapter (Nikon). The 488 excitation laser (Coherent) was set at 20 mW, and the 647 nm laser (Coherent) was set to 2 mW before being coupled into the Ti-TIRF optical fiber (Nikon). Two-color simultaneous imaging was performed by using a TuCAM (Andor) device that splits the emission onto two separate EMCCD cameras (Andor iXon 897). The excitation and emission were split by a quad band dichroic (Semrock), and the emission was further split by an FF640 filter (Semrock) and further filtered with an FF01-550/88 (Semrock) for the 488 channel and an FF01-642/LP (Semrock) for the 640 channel. The TuCAM imaging system introduces an extra 2 $\times$  magnification, yielding a final pixel size of 77 nm. The images from the two cameras were aligned by first imaging a grid of spots (Nanogrid MiralomaTech) on each camera and using the GridAligner plug-in for ImageJ.

DIC illumination was provided by a SOLA-SE-II (Lumencor) coupled to the microscope by a liquid light guide. A standard set of polarizer and analyzer (Nikon 100 X-II High NA/Oil) prisms was used, and the image was captured on a CoolSNAP (Photometrics) camera. The final pixel size for DIC images was 65 nm. Raw DIC images were processed using an FFT band-pass filter. DIC images were scaled and transformed to overlay with fluorescent images by imaging fluorescent microtubules in both channels for image registration. The entire imaging setup was controlled by Micro-Manager (66).

For data shown in figs. S3 and S4, images were analyzed using scripts in ImageJ and MATLAB. First, the offset between 640 and 488 channels was corrected with the GridAligner plug-in. Then microtubules were selected with 7 px-wide line

selection, and line scans were generated. These line scans were imported into a MATLAB script that identified the peaks in the 488 channel and recorded the number, intensity, and FWHM of the repair sites. The FWHM for a diffraction-limited spot was obtained by using 100-nm TetraSpeck beads (Thermo Fischer Scientific). Data were exported to Prism software for graphing.

#### **Transmission electron microscopy of microtubules repaired with recombinant tubulin**

GMPCPP-microtubules at 1  $\mu$ M concentration in 1 $\times$  BRB80 were applied to parafilm in a humidity chamber and incubated with 20 nM spastin in enzyme buffer [20 mM HEPES (pH 7.5), 300 mM KCl, 10 mM  $\text{MgCl}_2$ , 1 mM TCEP, and 0.5 mM ATP]. Buffer containing 0.5 mM ATP- $\gamma$ -S instead of ATP was used as a control. Severing was allowed to proceed for 30 s, followed by the addition of 0.6  $\mu$ M soluble FLAG-tagged single-isoform recombinant neuronal human  $\alpha$ 1A $\beta$ III tubulin to repair the microtubule lattice in the presence of 1 mM GTP and 5 mM ADP to inactivate the enzyme. The repair reaction was carried out for 5 min. Microtubules were then stabilized by the addition of 5 volumes of 0.2% glutaraldehyde in 1 $\times$  BRB80 (80 mM PIPES, 1 mM  $\text{MgCl}_2$ , 1 mM EGTA). After 3 min, cross-linking was quenched by the addition of Tris-HCl (pH 7.5) to a 20 mM final concentration and cross-linked microtubules were transferred into a 10-ml centrifuge tube (Beckman Coulter). The microtubule severing and healing procedure was repeated three more times, reaction mixtures were pooled into the same centrifuge tube, and microtubules were then spun down in an MLA-80 rotor at 100,000  $\times$  g for 15 min at 30°C. The microtubule pellet was gently washed with 200  $\mu$ l of 1 $\times$  BRB80 at 37°C twice and resuspended in 50  $\mu$ l of warm 1 $\times$  BRB80. Five microliters of 6.7  $\mu$ M monoclonal mouse-raised anti-FLAG M2 antibody (Sigma-Aldrich) and 5  $\mu$ l of 11.45  $\mu$ M goat anti-mouse antibody conjugated to 4-nm spherical gold nanoparticles, C11-4-TGAMG-50 (Nanopartz), were added to microtubules to label repaired sites. Antibody labeling was allowed to proceed for 5 min, and the reaction was mixed with 10 volumes of 30% glycerol in 1 $\times$  BRB80. Microtubules in 30% glycerol were loaded onto a 1 $\times$  BRB80 cushion containing 40% glycerol and spun down onto glow-discharged carbon-coated grids (carbon film only on 400 mesh; Ted Pella) at 4200  $\times$  g for 20 min at 30°C. Excess liquid was blotted with filter paper. Grids were washed three times with 30  $\mu$ l of BRB80, stained with 0.75% (w/v) uranyl formate, and air-dried. Images were collected on a T12 Technai electron microscope (FEI) equipped with a 2k  $\times$  2k Gatan US1000 CCD camera. Images were collected at nominal magnifications of 6800 $\times$  and 18,500 $\times$ , corresponding to pixel sizes of 6.8  $\text{\AA}/\text{pix}$  and 2.5  $\text{\AA}/\text{pix}$ , respectively. Images in fig. S7F were collected on a TF20 electron microscope (FEI) equipped with a K2 camera (Gatan). Images were collected at 50,000 $\times$  and 9600 $\times$  magnifications, corresponding to pixel sizes of 0.73  $\text{\AA}/\text{pix}$  and 3.65  $\text{\AA}/\text{pix}$ , respectively.

### Live imaging of severing and tubulin incorporation into nanoscale-damaged GMPCPP-microtubules and GMPCPP-capped GDP-microtubules

To observe microtubule severing and tubulin incorporation at damage sites simultaneously (Fig. 3 and fig. S5, A to C), GMPCPP-stabilized double-cycled microtubules labeled with 1% biotin and 20% HiLyte 647-tubulin were immobilized in imaging chambers. Image acquisition was started by using 100-ms continuous exposure in the 647 and 488 channels simultaneously, and the chamber was perfused with severing buffer containing 0.5 mM GTP, 20 nM spastin, and 0, 0.1, or 2  $\mu$ M HiLyte 488-labeled tubulin. Severing rates were calculated by manual counting of severing events (microtubule breaks) as a function of time. Tubulin incorporation sites were readily visible in the 488 channel. To observe the live incorporation of single tubulin dimers into microtubules damaged by spastin (Fig. 3, F and G), double-cycled GMPCPP-microtubules composed of 20% HiLyte 647-labeled and 1% biotinylated tubulin were immobilized in imaging chambers as described above. The chamber was then perfused with severing buffer, and images of microtubules were acquired. Microtubules were then incubated for 30 s with 20 nM spastin in severing buffer. Image acquisition was started during the spastin incubation step, and a solution containing fluorescently labeled tubulin [50 nM Alexa 488-labeled tubulin (PurSolutions) in BRB80 with 2-mg/ml casein, 14.3 mM 2-mercaptoethanol, 50 mM KCl, 2.5 mM  $MgCl_2$ , 1 mM ADP, 0.5 mM GTP, 1% Pluronic F127, and oxygen scavengers] was flushed in. Images were acquired for 5 min at 10 Hz in the 488-nm channel. After tubulin perfusion, the 640 laser was turned off to prevent photobleaching and microtubule photodamage. Images of fluorescent tubulin molecules landing on the microtubule were analyzed by using a  $7 \times 7$  pixel box, and the intensity of tubulin molecules incorporated into the microtubule was calibrated against the intensity of single tubulin dimers obtained by immobilizing 0.5 nM Alexa 488-tubulin on glass with an anti- $\beta$ -tubulin antibody (SAP.4G5; Sigma-Aldrich) and imaging under the same conditions.

For imaging of nonstabilized GDP-microtubules with a GMPCPP cap, sea urchin axonemes purified as described previously (67) were nonspecifically adhered to the coverslip, and 15  $\mu$ M tubulin containing 20% HiLyte 647-tubulin and 1 mM GTP were added to start microtubule growth from the axonemes. After the desired microtubule length (10 to 20  $\mu$ m) was achieved, the solution was exchanged quickly to introduce HiLyte 488-tubulin (20%) and 0.5 mM GMPCPP. After the growth of the GMPCPP cap, tubulin and nucleotide were washed out and spastin (5 nM) was introduced into the chamber with 1 mM ATP in the absence or presence of soluble tubulin at 2  $\mu$ M (500 nM HiLyte 488-tubulin + 1.5  $\mu$ M unlabeled tubulin) or 5  $\mu$ M (500 nM HiLyte 488-tubulin + 4.5  $\mu$ M unlabeled tubulin) and 0.5 mM GTP. Polymerization and imaging were performed at 30°C.

### Microtubule dynamics measurements and EB1 recognition of lattice-incorporated GTP-tubulin

TIRF microscopy chambers were prepared as described above. HiLyte 647 (10%)–labeled microtubules were polymerized at 30°C at 10  $\mu$ M tubulin. The chamber was perfused with 25 nM spastin or katanin and 10  $\mu$ M porcine brain tubulin containing 10% HiLyte 647-labeled tubulin in severing assay buffer (50 mM KCl, 1% Pluronic F127, 0.2-mg/ml casein, 6.2 mM 2-mercaptoethanol, 1.5% glycerol, 0.1% methylcellulose 4000cP, and oxygen scavengers in  $1 \times$  BRB80) with 1 mM GTP and 1 mM ATP together with 50 nM EB1-GFP. Images were acquired in the 647 and 488 channels simultaneously at 2 Hz. Microtubule rescues are defined as the transition of microtubules from shrinkage to growth. Rescue frequency was calculated as the number of rescues divided by the time spent depolymerizing. Catastrophes are defined as the transition of microtubules from growth to shrinkage. Catastrophe frequency was calculated as the number of catastrophes divided by the time spent in the polymerization state. The EB1 puncta and the microtubule rescue site were considered colocalized when the distance between the EB1 spot and the end of the depolymerizing microtubule was less than two pixels. The cutoff for an EB1 punctum was defined as having a mean intensity in a  $5 \times 5$  pixel box that is at least 3 standard deviations above the mean background EB1 lattice intensity. Background EB1 lattice intensity was determined from control chambers without severing enzymes. Background EB1 lattice intensity was the same in the absence of severing enzymes or the presence of severing enzymes but in the absence of ATP. For statistical significance calculation, rescue site analysis was also performed by using synthetic data generated by shifting the position of the EB1 spots by 7 pixels on the microtubule (alternatively, both toward the plus and the minus ends).

For the GTP-tubulin and EB1-GFP colocalization experiments shown in Fig. 6E, microtubule extensions were grown in the absence of fluorescent tubulin for 8 min at 30°C at 12  $\mu$ M porcine brain tubulin (Cytoskeleton) in severing assay buffer. The chamber was perfused with 20 nM spastin, 50 nM EB1-GFP, and 12  $\mu$ M porcine brain tubulin containing 10% HiLyte 647-labeled tubulin in severing assay buffer. Image acquisition was started during perfusion in the 640 and 488 channels simultaneously at 5 Hz. The offset between the 640 and 488 channels was corrected by using a nanogrid (Nanogrid Miraloma Tech) and the GridAligner plug-in in ImageJ.

### Laser ablation of microtubules with spastin- or katanin-generated GMPCPP islands

GMPCPP-stabilized unmodified microtubule seeds were immobilized on glass. To pregrow microtubules, 16  $\mu$ M tubulin containing 12.5% HiLyte 647-labeled tubulin with 1 mM GTP was perfused into the chamber and incubated for 10 min at 30°C. Microtubules were then capped using 6  $\mu$ M tubulin with 10% HiLyte 647 and 0.5 mM

GMPCPP. The chamber was washed after 2 min with severing assay buffer without GTP and then incubated with 4 nM spastin and 6  $\mu$ M tubulin containing 25% HiLyte 488-labeled tubulin in the presence of 200  $\mu$ M GMPCPP in severing assay buffer (50 mM KCl, 1% Pluronic F127, 0.2-mg/ml casein, 6.2 mM 2-mercaptoethanol, 2.5% glycerol, 0.1% methylcellulose 4000cP, and oxygen scavengers in  $1 \times$  BRB80) with or without 1 mM ATP for 3 min. The chamber was washed with buffer containing severing assay buffer. Microtubules were ablated with a 405-nm laser at 40% power using the iLas laser illuminator (BioVision). Images in the 488 and 647 channels were acquired sequentially with 100-ms exposure. For the rescue frequency measurements, 15% HiLyte 647-labeled tubulin at 7  $\mu$ M in severing assay buffer containing 1 mM GTP was perfused into the chamber. For the katanin experiments, the chamber was washed after microtubule capping with severing assay buffer without GTP and then incubated with 20 nM katanin and 8  $\mu$ M tubulin containing 25% HiLyte 488-labeled tubulin in the presence of 200  $\mu$ M GMPCPP in severing assay buffer with or without ATP for 45 s. Microtubule depolymerization rates through the GMPCPP islands were determined by dividing the length of the island by the time it takes to depolymerize through it.

### Laser ablation of dynamic microtubules with enzyme-generated GTP islands

TIRF microscopy chambers were prepared as described above. HiLyte 647-labeled microtubule extensions were polymerized for 8 min at 30°C at 12  $\mu$ M porcine brain tubulin (Cytoskeleton) containing 20% HiLyte 647-labeled tubulin in severing assay buffer. The chamber was perfused with 25 nM spastin or katanin, 50 nM EB1-GFP, and 12  $\mu$ M porcine brain tubulin containing 20% HiLyte 647-labeled tubulin in severing assay buffer with ATP or ATP- $\gamma$ -S. Microtubules were ablated by using a DeltaVision OMX with the 405-nm laser at 100% power for 1 s or with a 405-nm laser at 40% power using an iLas laser illuminator (BioVision). Images were acquired in the 647 and 488 channels at 5 Hz on the DeltaVision OMX and 2.9 Hz on the iLas system.

### Live imaging of tubulin incorporation and severing into dynamic microtubules

Chambers for TIRF microscopy were prepared as described above. GMPCPP-stabilized, unmodified microtubules containing 2% biotinylated tubulin were immobilized with 0.1-mg/ml NeutrAvidin (Thermo Fisher Scientific). Microtubule extensions were polymerized for 12 min at 30°C at 10 or 12  $\mu$ M porcine brain tubulin (Cytoskeleton) containing 10% HiLyte 647-tubulin in severing assay buffer (50 mM KCl, 1% Pluronic F127, 1 mM ATP, 1 mM GTP, 0.2-mg/ml casein, 6.2 mM 2-mercaptoethanol, 1.5% glycerol, 0.1% methylcellulose 4000cP, and oxygen scavengers in  $1 \times$  BRB80). Then, 25 nM katanin or spastin with 12  $\mu$ M porcine brain tubulin containing 10% HiLyte 488-labeled tubulin was perfused into the chamber in severing assay buffer. Images were acquired with 488 and 640 lasers simultaneously

at 2 Hz at 100-ms exposure. The incorporation of the HiLyte 488-tubulin was immediately visible upon perfusion only at microtubule tips in the control and along the microtubules and the dynamic tips in the enzyme and ATP conditions. Total polymer mass was obtained by measuring the background-corrected total integrated fluorescence in both the 488 and 640 channels. The laser ablation controls were performed at the same enzyme and tubulin concentrations but with 1 mM ATP- $\gamma$ -S. Microtubules were ablated with a 405-nm laser at 40% power using an iLas laser illuminator (BioVision) for the katanin experiments and the DeltaVision OMX for spastin.

### Quantification and data analysis

*n* numbers and statistical tests are reported for all experiments in the figure legends. All experiments were performed multiple times, and only representative images are shown. ImageJ was used for image analysis. Prism (GraphPad) was used for graphing and statistical analysis.

### REFERENCES AND NOTES

1. A. Roll-Mecak, F. J. McNally, Microtubule-severing enzymes. *Curr. Opin. Cell Biol.* **22**, 96–103 (2010). doi: [10.1016/j.cub.2009.11.001](https://doi.org/10.1016/j.cub.2009.11.001); pmid: [19963362](https://pubmed.ncbi.nlm.nih.gov/19963362/)
2. N. T. Sherwood, Q. Sun, M. Xue, B. Zhang, K. Zinn, *Drosophila* spastin regulates synaptic microtubule networks and is required for normal motor function. *PLoS Biol.* **2**, e429 (2004). doi: [10.1371/journal.pbio.0020429](https://doi.org/10.1371/journal.pbio.0020429); pmid: [15562320](https://pubmed.ncbi.nlm.nih.gov/15562320/)
3. N. Trotta, G. Orso, M. G. Rossetto, A. Daga, K. Broadie, The hereditary spastic paraplegia gene, *spastin*, regulates microtubule stability to modulate synaptic structure and function. *Curr. Biol.* **14**, 1135–1147 (2004). doi: [10.1016/j.cub.2004.06.058](https://doi.org/10.1016/j.cub.2004.06.058); pmid: [15242610](https://pubmed.ncbi.nlm.nih.gov/15242610/)
4. M. C. Stone et al., Normal *spastin* gene dosage is specifically required for axon regeneration. *Cell Rep.* **2**, 1340–1350 (2012). doi: [10.1016/j.celrep.2012.09.032](https://doi.org/10.1016/j.celrep.2012.09.032); pmid: [23122959](https://pubmed.ncbi.nlm.nih.gov/23122959/)
5. F. J. Ahmad, W. Yu, F. J. McNally, P. W. Baas, An essential role for katanin in severing microtubules in the neuron. *J. Cell Biol.* **145**, 305–315 (1999). doi: [10.1083/jcb.145.2.305](https://doi.org/10.1083/jcb.145.2.305); pmid: [10209026](https://pubmed.ncbi.nlm.nih.gov/10209026/)
6. V. Stoppin-Mellet, J. Gaillard, M. Vantard, Katanin's severing activity favors bundling of cortical microtubules in plants. *Plant J.* **46**, 1009–1017 (2006). doi: [10.1111/j.1365-313X.2006.02761.x](https://doi.org/10.1111/j.1365-313X.2006.02761.x); pmid: [16805733](https://pubmed.ncbi.nlm.nih.gov/16805733/)
7. Q. Zhang, E. Fishel, T. Bertrouche, R. Dixit, Microtubule severing at crossover sites by katanin generates ordered cortical microtubule arrays in *Arabidopsis*. *Curr. Biol.* **23**, 2191–2195 (2013). doi: [10.1016/j.cub.2013.09.018](https://doi.org/10.1016/j.cub.2013.09.018); pmid: [24206847](https://pubmed.ncbi.nlm.nih.gov/24206847/)
8. J. J. Lindeboom et al., A mechanism for reorientation of cortical microtubule arrays driven by microtubule severing. *Science* **342**, 1245533 (2013). doi: [10.1126/science.1245533](https://doi.org/10.1126/science.1245533); pmid: [24200811](https://pubmed.ncbi.nlm.nih.gov/24200811/)
9. D. Zhang, G. C. Rogers, D. W. Buster, D. J. Sharp, Three microtubule severing enzymes contribute to the "Pacman-flux" machinery that moves chromosomes. *J. Cell Biol.* **177**, 231–242 (2007). doi: [10.1083/jcb.200612011](https://doi.org/10.1083/jcb.200612011); pmid: [17452528](https://pubmed.ncbi.nlm.nih.gov/17452528/)
10. K. McNally, A. Audhya, K. Oegema, F. J. McNally, Katanin controls mitotic and meiotic spindle length. *J. Cell Biol.* **175**, 881–891 (2006). doi: [10.1083/jcb.200608117](https://doi.org/10.1083/jcb.200608117); pmid: [17178907](https://pubmed.ncbi.nlm.nih.gov/17178907/)
11. R. Loughlin, J. D. Wilbur, F. J. McNally, F. J. Nédélec, R. Heald, Katanin contributes to interspecies spindle length scaling in *Xenopus*. *Cell* **147**, 1397–1407 (2011). doi: [10.1016/j.cell.2011.11.014](https://doi.org/10.1016/j.cell.2011.11.014); pmid: [22153081](https://pubmed.ncbi.nlm.nih.gov/22153081/)
12. K. McNally et al., Katanin maintains meiotic metaphase chromosome alignment and spindle structure in vivo and has multiple effects on microtubules in vitro. *Mol. Biol. Cell* **25**, 1037–1049 (2014). doi: [10.1091/mbc.e13-12-0764](https://doi.org/10.1091/mbc.e13-12-0764); pmid: [24501424](https://pubmed.ncbi.nlm.nih.gov/24501424/)
13. N. Sharma et al., Katanin regulates dynamics of microtubules and biogenesis of motile cilia. *J. Cell Biol.* **178**, 1065–1079 (2007). doi: [10.1083/jcb.200704021](https://doi.org/10.1083/jcb.200704021); pmid: [17846175](https://pubmed.ncbi.nlm.nih.gov/17846175/)
14. W. F. Hu et al., Katanin p80 regulates human cortical development by limiting centriole and cilia number. *Neuron* **84**, 1240–1257 (2014). doi: [10.1016/j.neuron.2014.12.017](https://doi.org/10.1016/j.neuron.2014.12.017); pmid: [25521379](https://pubmed.ncbi.nlm.nih.gov/25521379/)
15. K. Mishra-Gorur et al., Mutations in KATNB1 cause complex cerebral malformations by disrupting asymmetrically dividing neural progenitors. *Neuron* **84**, 1226–1239 (2014). doi: [10.1016/j.neuron.2014.12.014](https://doi.org/10.1016/j.neuron.2014.12.014); pmid: [25521378](https://pubmed.ncbi.nlm.nih.gov/25521378/)
16. J. W. Connell, C. Lindon, J. P. Luzio, E. Reid, Spastin couples microtubule severing to membrane traffic in completion of cytokinesis and secretion. *Traffic* **10**, 42–56 (2009). doi: [10.1111/j.1600-0854.2008.00847.x](https://doi.org/10.1111/j.1600-0854.2008.00847.x); pmid: [19000169](https://pubmed.ncbi.nlm.nih.gov/19000169/)
17. J. Guizetti et al., Cortical constriction during abscission involves helices of ESCRT-III-dependent filaments. *Science* **331**, 1616–1620 (2011). doi: [10.1126/science.1201847](https://doi.org/10.1126/science.1201847); pmid: [21310966](https://pubmed.ncbi.nlm.nih.gov/21310966/)
18. A. Karabay, W. Yu, J. M. Solowska, D. H. Baird, P. W. Baas, Axonal growth is sensitive to the levels of katanin, a protein that severs microtubules. *J. Neurosci.* **24**, 5778–5788 (2004). doi: [10.1523/JNEUROSCI.1382-04.2004](https://doi.org/10.1523/JNEUROSCI.1382-04.2004); pmid: [15215300](https://pubmed.ncbi.nlm.nih.gov/15215300/)
19. R. A. Charafeddine et al., Fidgetin-Like 2: A microtubule-based regulator of wound healing. *J. Invest. Dermatol.* **135**, 2309–2318 (2015). doi: [10.1038/jid.2015.94](https://doi.org/10.1038/jid.2015.94); pmid: [25756798](https://pubmed.ncbi.nlm.nih.gov/25756798/)
20. G. Yigit et al., A syndrome of microcephaly, short stature, polysyndactyly, and dental anomalies caused by a homozygous KATNB1 mutation. *Am. J. Med. Genet. A* **170**, 728–733 (2016). doi: [10.1002/ajmg.a.37484](https://doi.org/10.1002/ajmg.a.37484); pmid: [26640080](https://pubmed.ncbi.nlm.nih.gov/26640080/)
21. A. Roll-Mecak, R. D. Vale, The *Drosophila* homologue of the hereditary spastic paraplegia protein, spastin, severs and disassembles microtubules. *Curr. Biol.* **15**, 650–655 (2005). doi: [10.1016/j.cub.2005.02.029](https://doi.org/10.1016/j.cub.2005.02.029); pmid: [15823537](https://pubmed.ncbi.nlm.nih.gov/15823537/)
22. K. Jiang et al., Microtubule minus-end regulation at spindle poles by an ASPM-katanin complex. *Nat. Cell Biol.* **19**, 480–492 (2017). doi: [10.1038/ncb3511](https://doi.org/10.1038/ncb3511); pmid: [28436967](https://pubmed.ncbi.nlm.nih.gov/28436967/)
23. J. D. Wood et al., The microtubule-severing protein Spastin is essential for axon outgrowth in the zebrafish embryo. *Hum. Mol. Genet.* **15**, 2763–2771 (2006). doi: [10.1093/hmg/ddl212](https://doi.org/10.1093/hmg/ddl212); pmid: [16893913](https://pubmed.ncbi.nlm.nih.gov/16893913/)
24. D. H. Burk, Z.-H. Ye, Alteration of oriented deposition of cellulose microfibrils by mutation of a katanin-like microtubule-severing protein. *Plant Cell* **14**, 2145–2160 (2002). doi: [10.1105/tpc.003947](https://doi.org/10.1105/tpc.003947); pmid: [12215512](https://pubmed.ncbi.nlm.nih.gov/12215512/)
25. M. Srayko, E. T. O'toole, A. A. Hyman, T. Müller-Reichert, Katanin disrupts the microtubule lattice and increases polymer number in *C. elegans* meiosis. *Curr. Biol.* **16**, 1944–1949 (2006). doi: [10.1016/j.cub.2006.08.029](https://doi.org/10.1016/j.cub.2006.08.029); pmid: [17027492](https://pubmed.ncbi.nlm.nih.gov/17027492/)
26. K. Ribbeck, T. J. Mitchison, Meiotic spindle: Sculpted by severing. *Curr. Biol.* **16**, R923–R925 (2006). doi: [10.1016/j.cub.2006.09.048](https://doi.org/10.1016/j.cub.2006.09.048); pmid: [17084690](https://pubmed.ncbi.nlm.nih.gov/17084690/)
27. A. Roll-Mecak, R. D. Vale, Making more microtubules by severing: A common theme of noncentrosomal microtubule arrays? *J. Cell Biol.* **175**, 849–851 (2006). doi: [10.1083/jcb.200611149](https://doi.org/10.1083/jcb.200611149); pmid: [17178905](https://pubmed.ncbi.nlm.nih.gov/17178905/)
28. R. A. Walker, S. Inoué, E. D. Salmon, Asymmetric behavior of severed microtubule ends after ultraviolet-microbeam irradiation of individual microtubules in vitro. *J. Cell Biol.* **108**, 931–937 (1989). doi: [10.1083/jcb.108.3.931](https://doi.org/10.1083/jcb.108.3.931); pmid: [2921286](https://pubmed.ncbi.nlm.nih.gov/2921286/)
29. P. T. Tran, R. A. Walker, E. D. Salmon, A metastable intermediate state of microtubule dynamic instability that differs significantly between plus and minus ends. *J. Cell Biol.* **138**, 105–117 (1997). doi: [10.1083/jcb.138.1.105](https://doi.org/10.1083/jcb.138.1.105); pmid: [9214385](https://pubmed.ncbi.nlm.nih.gov/9214385/)
30. T. Mitchison, M. Kirschner, Dynamic instability of microtubule growth. *Nature* **312**, 237–242 (1984). doi: [10.1038/312237a0](https://doi.org/10.1038/312237a0); pmid: [6504138](https://pubmed.ncbi.nlm.nih.gov/6504138/)
31. M. F. Carlier, D. Pantaloni, Kinetic analysis of guanosine 5'-triphosphate hydrolysis associated with tubulin polymerization. *Biochemistry* **20**, 1918–1924 (1981). doi: [10.1021/bi00510a030](https://doi.org/10.1021/bi00510a030); pmid: [7225365](https://pubmed.ncbi.nlm.nih.gov/7225365/)
32. D. Zhang et al., *Drosophila* katanin is a microtubule depolymerase that regulates cortical-microtubule plus-end interactions and cell migration. *Nat. Cell Biol.* **13**, 361–370 (2011). doi: [10.1038/ncb2206](https://doi.org/10.1038/ncb2206); pmid: [21378981](https://pubmed.ncbi.nlm.nih.gov/21378981/)
33. L. Schaedel et al., Microtubules self-repair in response to mechanical stress. *Nat. Mater.* **14**, 1156–1163 (2015). doi: [10.1038/nmat4396](https://doi.org/10.1038/nmat4396); pmid: [26343914](https://pubmed.ncbi.nlm.nih.gov/26343914/)
34. C. Aumeier et al., Self-repair promotes microtubule rescue. *Nat. Cell Biol.* **18**, 1054–1064 (2016). doi: [10.1038/ncb3406](https://doi.org/10.1038/ncb3406); pmid: [27617929](https://pubmed.ncbi.nlm.nih.gov/27617929/)
35. M. E. Bailey, D. L. Sackett, J. L. Ross, Katanin severing and binding microtubules are inhibited by tubulin carboxy tails. *Biophys. J.* **109**, 2546–2561 (2015). doi: [10.1016/j.bpj.2015.11.011](https://doi.org/10.1016/j.bpj.2015.11.011); pmid: [26682813](https://pubmed.ncbi.nlm.nih.gov/26682813/)
36. G. Hiller, K. Weber, Radioimmunoassay for tubulin: A quantitative comparison of the tubulin content of different established tissue culture cells and tissues. *Cell* **14**, 795–804 (1978). doi: [10.1016/0092-8674\(78\)90335-5](https://doi.org/10.1016/0092-8674(78)90335-5); pmid: [688394](https://pubmed.ncbi.nlm.nih.gov/688394/)
37. D. N. Itzhak, S. Tyanova, J. Cox, G. H. Borner, Global, quantitative and dynamic mapping of protein subcellular localization. *eLife* **5**, e16950 (2016). doi: [10.7554/eLife.16950](https://doi.org/10.7554/eLife.16950); pmid: [27287775](https://pubmed.ncbi.nlm.nih.gov/27287775/)
38. A. Vemu et al., Structure and dynamics of single-isoform recombinant neuronal human tubulin. *J. Biol. Chem.* **291**, 12907–12915 (2016). doi: [10.1074/jbc.C116.731133](https://doi.org/10.1074/jbc.C116.731133); pmid: [27129203](https://pubmed.ncbi.nlm.nih.gov/27129203/)
39. M.-F. Carlier, Guanosine-5'-triphosphate hydrolysis and tubulin polymerization. *Mol. Cell. Biochem.* **47**, 97–113 (1982). doi: [10.1007/BF00234410](https://doi.org/10.1007/BF00234410); pmid: [6755216](https://pubmed.ncbi.nlm.nih.gov/6755216/)
40. M. F. Carlier, D. Pantaloni, Assembly of microtubule protein: Role of guanosine di- and triphosphate nucleotides. *Biochemistry* **21**, 1215–1224 (1982). doi: [10.1021/bi00535a017](https://doi.org/10.1021/bi00535a017); pmid: [7074077](https://pubmed.ncbi.nlm.nih.gov/7074077/)
41. M. F. Carlier, D. Didry, D. Pantaloni, Microtubule elongation and guanosine 5'-triphosphate hydrolysis. Role of guanine nucleotides in microtubule dynamics. *Biochemistry* **26**, 4428–4437 (1987). doi: [10.1021/bi00388a036](https://doi.org/10.1021/bi00388a036); pmid: [3663597](https://pubmed.ncbi.nlm.nih.gov/3663597/)
42. V. VanBuren, D. J. Odde, L. Cassimeris, Estimates of lateral and longitudinal bond energies within the microtubule lattice. *Proc. Natl. Acad. Sci. U.S.A.* **99**, 6035–6040 (2002). doi: [10.1073/pnas.092504999](https://doi.org/10.1073/pnas.092504999); pmid: [11983898](https://pubmed.ncbi.nlm.nih.gov/11983898/)
43. A. Dimitrov et al., Detection of GTP-tubulin conformation in vivo reveals a role for GTP remnants in microtubule rescues. *Science* **322**, 1353–1356 (2008). doi: [10.1126/science.1165401](https://doi.org/10.1126/science.1165401); pmid: [18927356](https://pubmed.ncbi.nlm.nih.gov/18927356/)
44. J. Al-Bassam et al., CLASP promotes microtubule rescue by recruiting tubulin dimers to the microtubule. *Dev. Cell* **19**, 245–258 (2010). doi: [10.1016/j.devcel.2010.07.016](https://doi.org/10.1016/j.devcel.2010.07.016); pmid: [20780887](https://pubmed.ncbi.nlm.nih.gov/20780887/)
45. K. Ichihara, H. Kitazawa, Y. Iguchi, H. Hotani, T. J. Itoh, Visualization of the stop of microtubule depolymerization that occurs at the high-density region of microtubule-associated protein 2 (MAP2). *J. Mol. Biol.* **312**, 107–118 (2001). doi: [10.1006/jmbi.2001.4934](https://doi.org/10.1006/jmbi.2001.4934); pmid: [11545589](https://pubmed.ncbi.nlm.nih.gov/11545589/)
46. M. Zanic, J. H. Stear, A. A. Hyman, J. Howard, EB1 recognizes the nucleotide state of tubulin in the microtubule lattice. *PLoS ONE* **4**, e7585 (2009). doi: [10.1371/journal.pone.0007585](https://doi.org/10.1371/journal.pone.0007585); pmid: [19851462](https://pubmed.ncbi.nlm.nih.gov/19851462/)
47. S. P. Maurer, F. J. Fournill, G. Bohner, C. A. Moores, T. Surrey, EBs recognize a nucleotide-dependent structural cap at growing microtubule ends. *Cell* **149**, 371–382 (2012). doi: [10.1016/j.cell.2012.02.049](https://doi.org/10.1016/j.cell.2012.02.049); pmid: [22500803](https://pubmed.ncbi.nlm.nih.gov/22500803/)
48. T. P. Spurrck et al., UV microbeam irradiations of the mitotic spindle. II. Spindle fiber dynamics and force production. *J. Cell Biol.* **111**, 1505–1518 (1990). doi: [10.1083/jcb.111.4.1505](https://doi.org/10.1083/jcb.111.4.1505); pmid: [2218123](https://pubmed.ncbi.nlm.nih.gov/2218123/)
49. J. Brugués, V. Nuzzo, E. Mazur, D. J. Needleman, Nucleation and transport organize microtubules in metaphase spindles. *Cell* **149**, 554–564 (2012). doi: [10.1016/j.cell.2012.03.027](https://doi.org/10.1016/j.cell.2012.03.027); pmid: [22541427](https://pubmed.ncbi.nlm.nih.gov/22541427/)
50. R. B. Nicklas, G. M. Lee, C. L. Rieder, G. Rupp, Mechanically cut mitotic spindles: Clean cuts and stable microtubules. *J. Cell Sci.* **94**, 415–423 (1989). pmid: [2698889](https://pubmed.ncbi.nlm.nih.gov/2698889/)
51. J. S. Tirnauer, E. D. Salmon, T. J. Mitchison, Microtubule plus-end dynamics in *Xenopus* egg extract spindles. *Mol. Biol. Cell* **15**, 1776–1784 (2004). doi: [10.1091/mbc.e03-11-0824](https://doi.org/10.1091/mbc.e03-11-0824); pmid: [14767058](https://pubmed.ncbi.nlm.nih.gov/14767058/)
52. J. Howard, A. A. Hyman, Microtubule polymerases and depolymerases. *Curr. Opin. Cell Biol.* **19**, 31–35 (2007). doi: [10.1016/j.cub.2006.12.009](https://doi.org/10.1016/j.cub.2006.12.009); pmid: [17184986](https://pubmed.ncbi.nlm.nih.gov/17184986/)
53. R. D. Vale, Severing of stable microtubules by a mitotically activated protein in *Xenopus* egg extracts. *Cell* **64**, 827–839 (1991). doi: [10.1016/0092-8674\(91\)90511-V](https://doi.org/10.1016/0092-8674(91)90511-V); pmid: [1671762](https://pubmed.ncbi.nlm.nih.gov/1671762/)
54. M. E. Bailey, M. M. Morelli, J. D. Diaz, J. L. Ross, Katanin P60 targets microtubules with defects. *Biophys. J.* **102**, 701a (2012). doi: [10.1016/j.bpj.2011.11.3806](https://doi.org/10.1016/j.bpj.2011.11.3806)
55. H. de Forges et al., Localized mechanical stress promotes microtubule rescue. *Curr. Biol.* **26**, 3399–3406 (2016). doi: [10.1016/j.cub.2016.10.048](https://doi.org/10.1016/j.cub.2016.10.048); pmid: [27916523](https://pubmed.ncbi.nlm.nih.gov/27916523/)
56. C. Wang et al., KTN80 confers precision to microtubule severing by specific targeting of katanin complexes in plant cells. *EMBO J.* **36**, 3435–3447 (2017). doi: [10.15252/emj.201796823](https://doi.org/10.15252/emj.201796823); pmid: [28978669](https://pubmed.ncbi.nlm.nih.gov/28978669/)
57. M. L. Valenstein, A. Roll-Mecak, Graded control of microtubule severing by tubulin glutamylation. *Cell* **164**, 911–921 (2016). doi: [10.1016/j.cell.2016.01.019](https://doi.org/10.1016/j.cell.2016.01.019); pmid: [26875866](https://pubmed.ncbi.nlm.nih.gov/26875866/)
58. B. Lacroix et al., Tubulin polyglutamylation stimulates spastin-mediated microtubule severing. *J. Cell Biol.* **189**, 945–954 (2010). doi: [10.1083/jcb.201001024](https://doi.org/10.1083/jcb.201001024); pmid: [20530212](https://pubmed.ncbi.nlm.nih.gov/20530212/)
59. T. Nakata, S. Niwa, Y. Okada, F. Perez, N. Hirokawa, Preferential binding of a kinesin-1 motor to GTP-tubulin-rich

- microtubules underlies polarized vesicle transport. *J. Cell Biol.* **194**, 245–255 (2011). doi: [10.1083/jcb.201104034](https://doi.org/10.1083/jcb.201104034); pmid: [21768290](https://pubmed.ncbi.nlm.nih.gov/21768290/)
60. A. Y. Chan, M. Bailly, N. Zebda, J. E. Segall, J. S. Condeelis, Role of cofilin in epidermal growth factor-stimulated actin polymerization and lamellipod protrusion. *J. Cell Biol.* **148**, 531–542 (2000). doi: [10.1083/jcb.148.3.531](https://doi.org/10.1083/jcb.148.3.531); pmid: [10662778](https://pubmed.ncbi.nlm.nih.gov/10662778/)
61. V. DesMarais, M. Ghosh, R. Eddy, J. Condeelis, Cofilin takes the lead. *J. Cell Sci.* **118**, 19–26 (2005). doi: [10.1242/jcs.01631](https://doi.org/10.1242/jcs.01631); pmid: [15615780](https://pubmed.ncbi.nlm.nih.gov/15615780/)
62. N. E. Ziótkowska, A. Roll-Mecak, In vitro microtubule severing assays. *Methods Mol. Biol.* **1046**, 323–334 (2013). doi: [10.1007/978-1-62703-538-5\\_19](https://doi.org/10.1007/978-1-62703-538-5_19); pmid: [23868597](https://pubmed.ncbi.nlm.nih.gov/23868597/)
63. E. Zehr *et al.*, Katanin spiral and ring structures shed light on power stroke for microtubule severing. *Nat. Struct. Mol. Biol.* **24**, 717–725 (2017). doi: [10.1038/nsmb.3448](https://doi.org/10.1038/nsmb.3448); pmid: [28783150](https://pubmed.ncbi.nlm.nih.gov/28783150/)
64. A. J. Albee, C. Wiese, Xenopus TACC3/maskin is not required for microtubule stability but is required for anchoring microtubules at the centrosome. *Mol. Biol. Cell* **19**, 3347–3356 (2008). doi: [10.1091/mbc.e07-11-1204](https://doi.org/10.1091/mbc.e07-11-1204); pmid: [18508920](https://pubmed.ncbi.nlm.nih.gov/18508920/)
65. C. Gell, C. T. Friel, B. Boronovo, D. N. Drechsel, A. A. Hyman, J. Howard, "Purification of tubulin from porcine brain," in *Microtubule Dynamics: Methods and Protocols*, A. Straube, Ed. (Springer, 2011), pp. 15–28.
66. A. D. Edelstein *et al.*, Advanced methods of microscope control using  $\mu$ Manager software. *J. Biol. Methods* **1**, e10 (2014). doi: [10.14440/jbm.2014.36](https://doi.org/10.14440/jbm.2014.36); pmid: [25606571](https://pubmed.ncbi.nlm.nih.gov/25606571/)
67. I. R. Gibbons, E. Fronk, A latent adenosine triphosphatase form of dynein 1 from sea urchin sperm flagella. *J. Biol. Chem.* **254**, 187–196 (1979). pmid: [214440](https://pubmed.ncbi.nlm.nih.gov/214440/)

#### ACKNOWLEDGMENTS

We thank A. Szyk, National Institute of Neurological Disorders and Stroke (NINDS), for purified spastin and katanin, and X. Wu, National Heart, Lung, and Blood Institute (NHLBI), for help in the Light Microscopy Core. **Funding:** N.G. is a Howard Hughes Medical Institute investigator. A.M.D. is supported by NIH grant R01GM121975. A.R.-M. is supported by the intramural programs of NINDS and NHLBI. **Author contributions:** A.V. performed TIRF experiments with dynamic microtubules and laser ablation. E.S. performed TIRF experiments with stabilized and dynamic microtubules. A.V., E.S., and J.O.S. performed image analysis. E.A.Z. performed EM time

courses with spastin and all EM experiments with katanin and recombinant tubulin. A.M.D. performed initial in-the-tube and on-grid EM experiments with spastin. A.M.D. and N.G. discussed EM experiments. A.R.-M. wrote the manuscript with input from A.M.D., E.S., A.V., and E.A.Z. All authors planned experiments and reviewed the manuscript. A.R.-M. conceived of the project, conceptualized the manuscript, and supervised research. **Competing interests:** The authors declare no competing financial interests. **Data and material availability:** All data needed to understand and assess the conclusions of this research are available in the main text and supplementary materials. Information requests and requests for reagents should be directed to the corresponding author.

#### SUPPLEMENTARY MATERIALS

[www.sciencemag.org/content/361/6404/eaau1504/suppl/DC1](http://www.sciencemag.org/content/361/6404/eaau1504/suppl/DC1)  
Figs. S1 to S10  
Movies S1 to S7

11 May 2018; accepted 18 July 2018  
10.1126/science.aau1504



## Supplementary Materials for

### **Severing enzymes amplify microtubule arrays through lattice GTP-tubulin incorporation**

Annapurna Vemu\*, Ewa Szczesna\*, Elena A. Zehr, Jeffrey O. Spector, Nikolaus Grigorieff, Alexandra M. Deaconescu, Antonina Roll-Mecak†

\*These authors contributed equally to this work.

†Corresponding author. Email: Antonina@mail.nih.gov

Published 24 August 2018, *Science* **361**, eaau1504 (2018)  
DOI: 10.1126/science.aau1504

#### **This PDF file includes:**

Figs. S1 to S10  
Captions for Movies S1 to S7  
References

**Other Supplementary Material for this manuscript includes the following:**  
(available at [www.sciencemag.org/content/361/6404/eaau1504/suppl/DC1](http://www.sciencemag.org/content/361/6404/eaau1504/suppl/DC1))

Movies S1 to S7

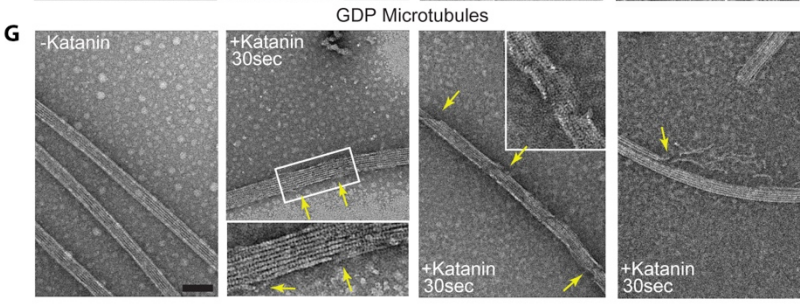
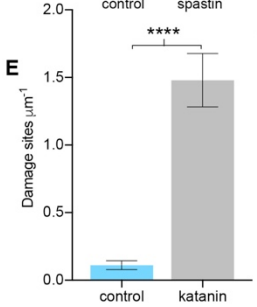
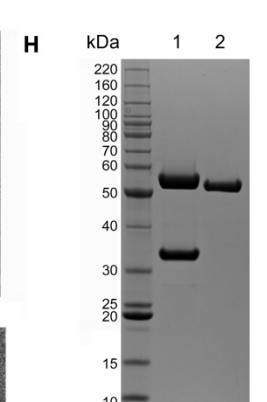
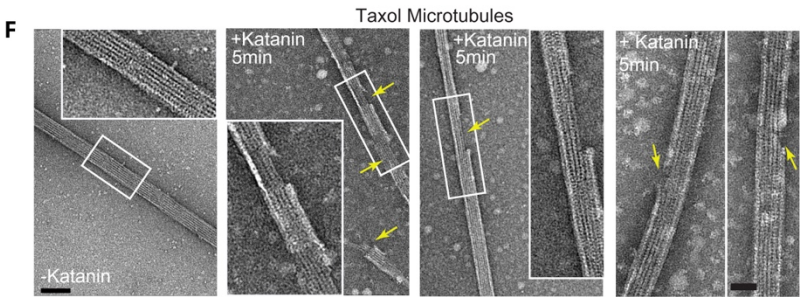
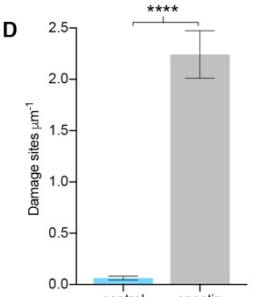
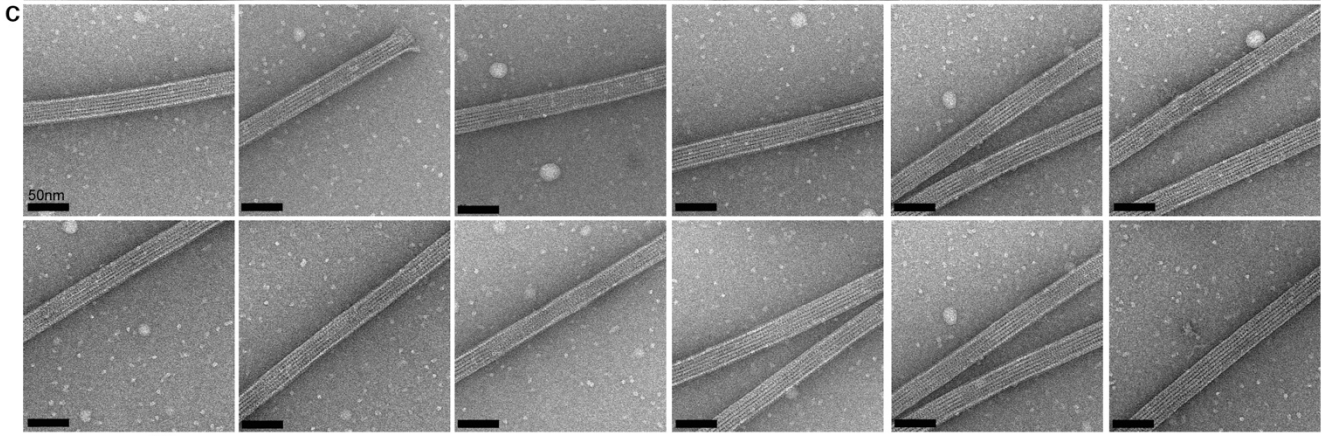
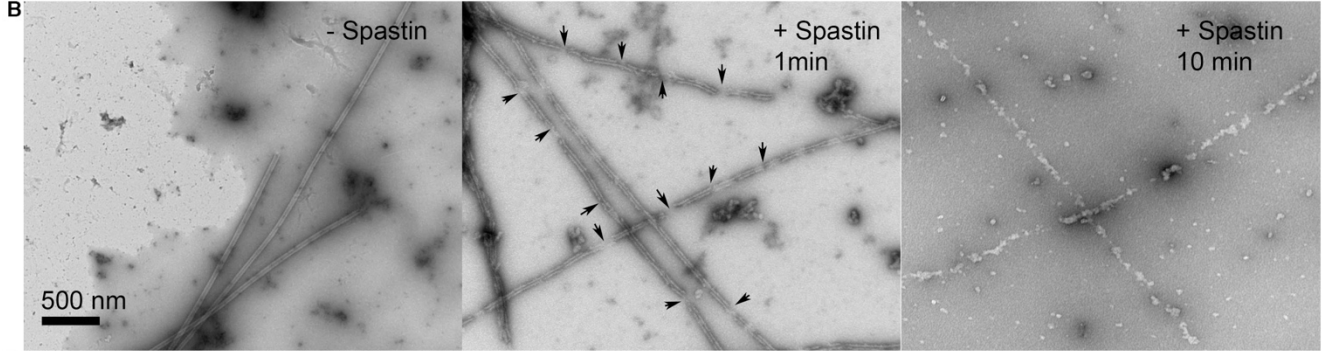
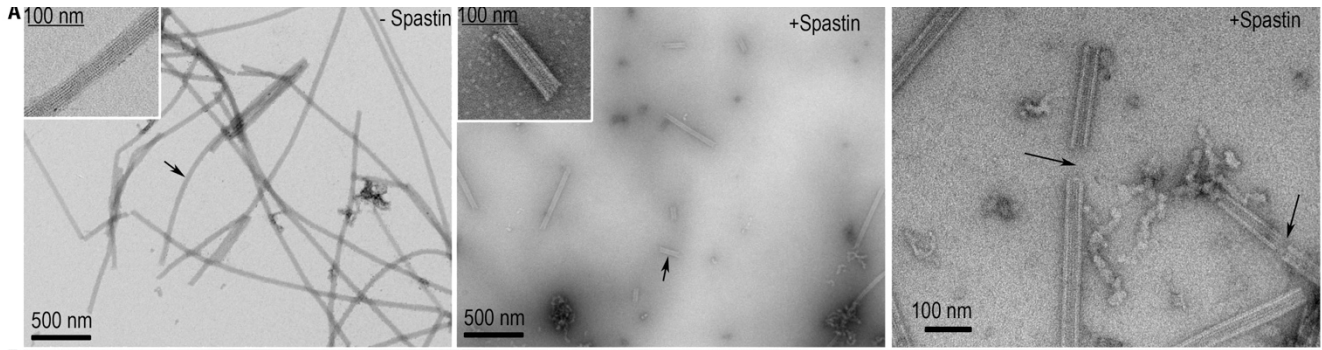


## Fig. S1.

### Transmission electron microscopy of spastin and katanin catalyzed microtubule-severing reactions

(A) Fields of taxol-stabilized microtubules in control buffer or after incubation with spastin in solution and pipetted onto EM grid. Microtubules imaged at 14,000x magnification. (B) Fields of taxol-stabilized microtubules in control buffer and in the presence of spastin negatively stained after 1 or 10 min of on-grid incubation (Materials and methods). Black arrows indicate severing sites. After prolonged incubation with spastin (right), the protofilament structure of the microtubule is gone, and a proteinaceous residue is left on the grid. (C) Fields of GMPCPP-stabilized microtubules in control buffer. Scale bar, 50 nm. Microtubules imaged at 30,000x magnification. (D) Frequency of nanoscale damage in control microtubules and microtubules treated with 25 nM spastin and 1 mM ATP for 5 min; 150 micrographs for the control and 100 micrographs analyzed for spastin +ATP (E) Frequency of nanoscale damage in control microtubules and microtubules treated with 100 nM katanin and 1 mM ATP for 5 min; 100 micrographs for the control and 112 micrographs analyzed for katanin + ATP; error bars, s.e.m.; \*\*\*\*, P values < 0.0001 determined by two-tailed t-test (F-G) Fields of taxol stabilized GDP microtubules (F) and GDP microtubules (G) incubated with buffer as control or katanin and ATP. Reactions were passively deposited on EM grids, negatively stained and visualized by TEM (Materials and methods). Arrows indicate nanoscale damage sites; Scale bar, 50 nm. Microtubules imaged at 13,000x magnification; boxed regions imaged at 30,000x magnification. (H) SDS gel showing bacterially expressed and purified katanin p60:p80 (lane 1) and spastin (lane 2) used in this study (Materials and methods); 5 and 2.5  $\mu$ g loaded for katanin and spastin, respectively.

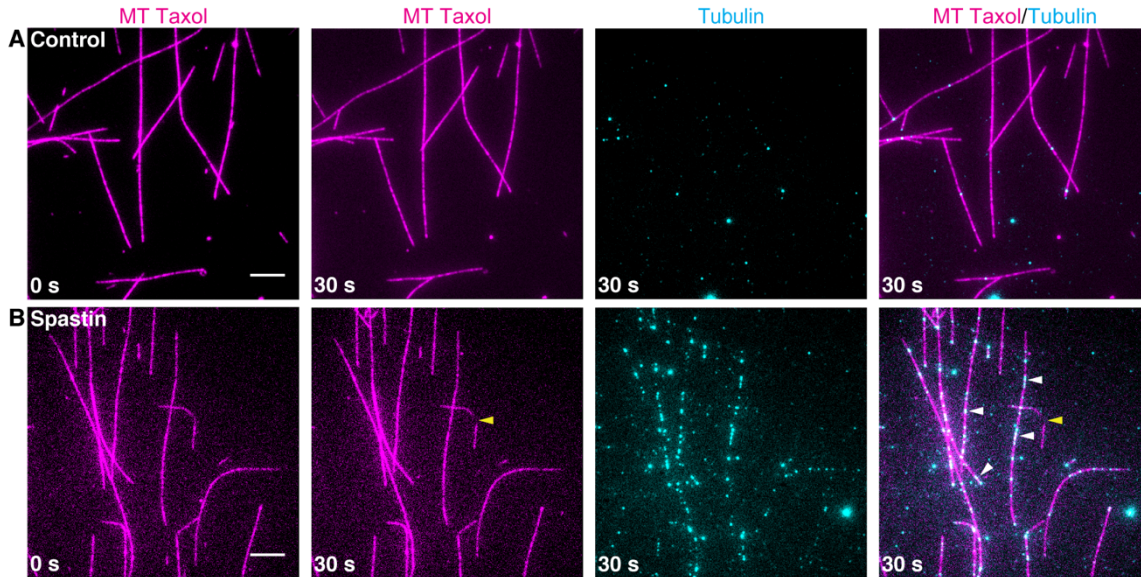


**Fig. S2.**

**Soluble tubulin incorporates into taxol-stabilized microtubules after spastin-induced nanoscale damage**

(A, B) Soluble tubulin incorporates into taxol-stabilized microtubules after spastin-induced nanoscale damage. HiLyte647-labeled taxol stabilized microtubules (magenta) incubated with buffer (A) or spastin (B) followed by incubation with 100 nM HiLyte488-labeled tubulin (cyan). The repair step was performed with 100 nM soluble tubulin to prevent microtubule nucleation in the presence of taxol. After 30 s incubation with spastin abundant tubulin incorporation (white arrows) is observed along the entire microtubule with few complete severing events detected (yellow arrows). Scale bar, 5  $\mu$ m.

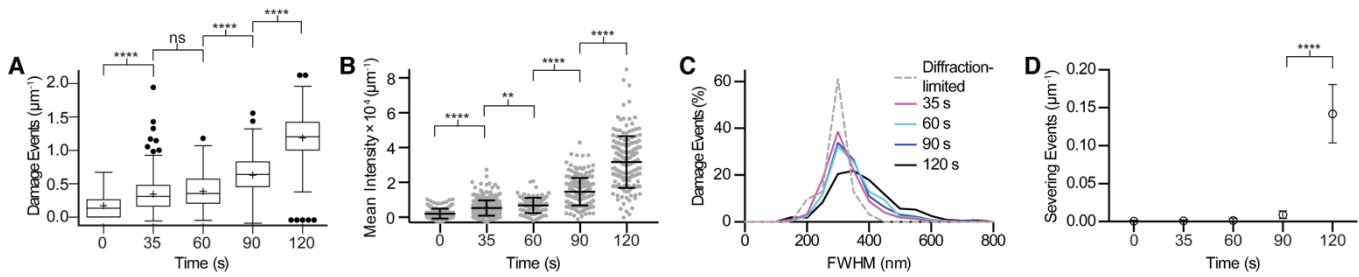


**Fig. S3.**

**Progressive spastin mediated nanoscale damage precedes the onset of microtubule severing.**

(A) Density of incorporated HiLyte488-labeled tubulin puncta along microtubules as a function of spastin incubation time;  $n = 188, 316, 100, 319$  and  $149$  microtubules from multiple chambers for 0, 35, 60, 90 and 120s, respectively. (B) Fluorescence intensity of incorporated HiLyte488-labeled tubulin puncta along microtubules as a function of spastin incubation time;  $n = 216, 385, 100, 201$  and  $161$  from multiple chambers for 0, 35, 60, 90 and 120s, respectively. Error bars indicate S.D. (C) Distribution of full-width-at-half-maximum (FWHM) of nanoscale damage sites as a function of spastin incubation time ( $n=1245, 398, 2457$  and  $971$  events for 35, 60, 90 and 120 s respectively). The dashed line shows FWHM for 100 nm TetraSpeck microspheres (Thermo Fisher Scientific). (D) Severing events (microtubule breaks) as a function of time ( $n=216, 385, 100, 161$  and  $201$  microtubules for control, 35, 60, 90, and 120 s respectively for data in panels A, B and D). Error bars, s.e.m. \*\*, P values  $< 0.01$ ; \*\*\*\*, P values  $< 0.0001$  determined by two-tailed t-test with Welch correction.

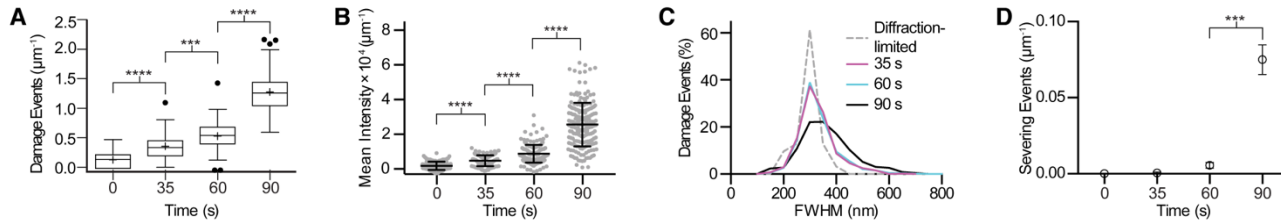


**Fig. S4.**

**Progressive katanin mediated microtubule nanoscale damage precedes the onset of severing.**

(A) Density of incorporated HiLyte488-labeled tubulin puncta along microtubules as a function of katanin incubation time;  $n = 57, 56, 45$  and  $91$  microtubules from multiple chambers for  $0, 35, 60,$  and  $90$ s, respectively. (B) HiLyte488 fluorescence intensity of incorporated HiLyte488-labeled tubulin puncta as a function of katanin incubation time;  $n = 144, 112, 177$  and  $192$  for  $0, 35, 60,$  and  $90$ s, respectively. Error bars indicate S.D. (C) Distribution of full-width-at-half-maximum (FWHM) of nanoscale damage sites as a function of katanin incubation time ( $n=519, 1246$  and  $1813$  events for  $35, 60$  and  $90$  s respectively). The dashed line shows FWHM for  $100$  nm TetraSpeck microspheres (Thermo Fisher Scientific). (D) Severing events (microtubule breaks) as a function of time ( $n=144, 112, 177$  and  $192$  microtubules for control,  $35, 60$  and  $90$  s respectively for data in panels (A), (B) and (D), respectively). Error bars, s.e.m.; \*\*\*, P values  $< 0.001$ , \*\*\*\*, P values  $< 0.0001$  determined by two-tailed t-test with Welch correction.

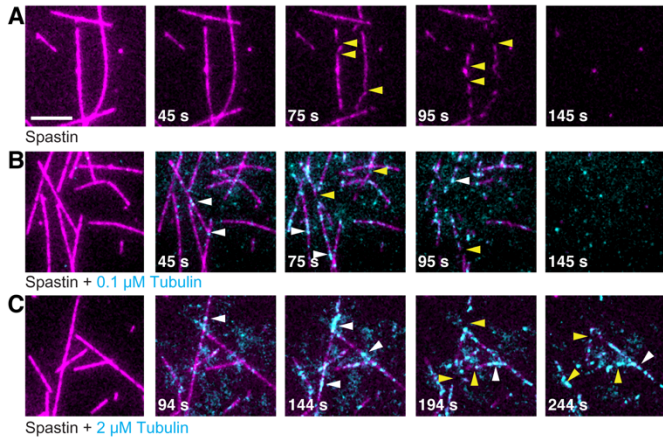


**Fig. S5.**

**Incorporation of soluble tubulin into spastin-induced nanoscale damage sites inhibits microtubule severing**

(A-C) Spastin induced microtubule severing in the absence of tubulin (A) or presence of 100 nM (B) and 2  $\mu$ M soluble HiLyte488-labeled tubulin (C). Microtubules (magenta), incorporated HiLyte488-labeled tubulin (cyan). White arrows indicate tubulin incorporation sites, yellow arrows, mesoscale severing events. Scale bar, 5  $\mu$ m.

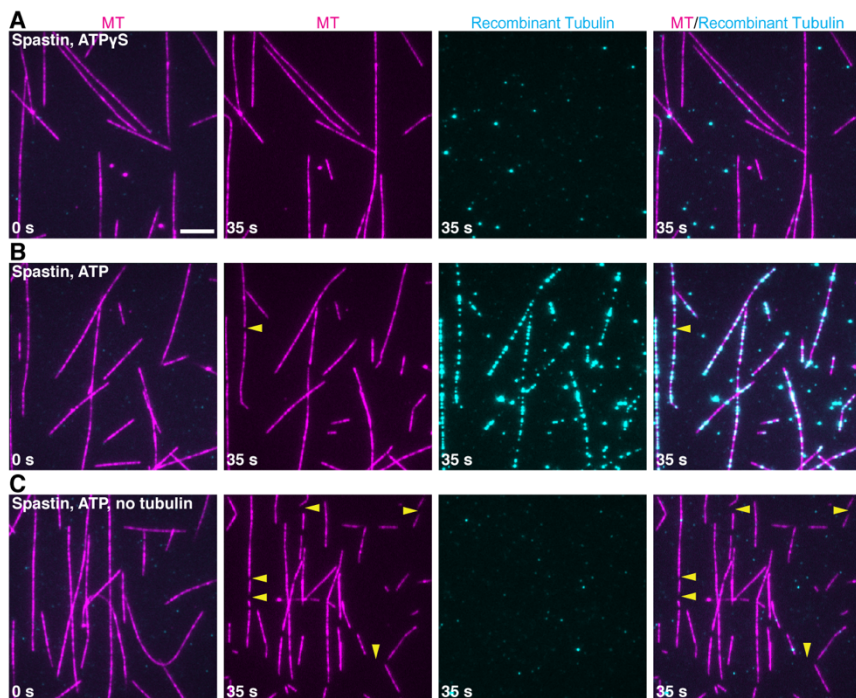


**Fig. S6.**

**Recombinant FLAG-tagged tubulin incorporates into microtubules damaged at the nanoscale by spastin**  
 (A–C) HiLyte647-labeled GMCPP brain microtubules (magenta) incubated with 10 nM spastin followed by incubation with 1  $\mu$ M recombinant human  $\alpha$ 1A/ $\beta$ III tubulin with a C-terminal FLAG tag on  $\beta$ III-tubulin (Materials and methods). The recombinant tubulin was detected by anti-FLAG antibodies and secondary Alexa488-labeled antibodies (cyan). Free tubulin does not incorporate into microtubules incubated with spastin and the non-hydrolyzable ATP analog ATP $\gamma$ S (A), while after 35 s incubation with spastin and ATP robust tubulin incorporation is observed along the entire length of the microtubule (B). Detection by the anti-FLAG antibodies is specific as there is no signal on microtubules damaged at the nanoscale by spastin and not incubated with recombinant tubulin (C). Yellow arrows indicate mesoscale severing events. Scale bar, 5  $\mu$ m.

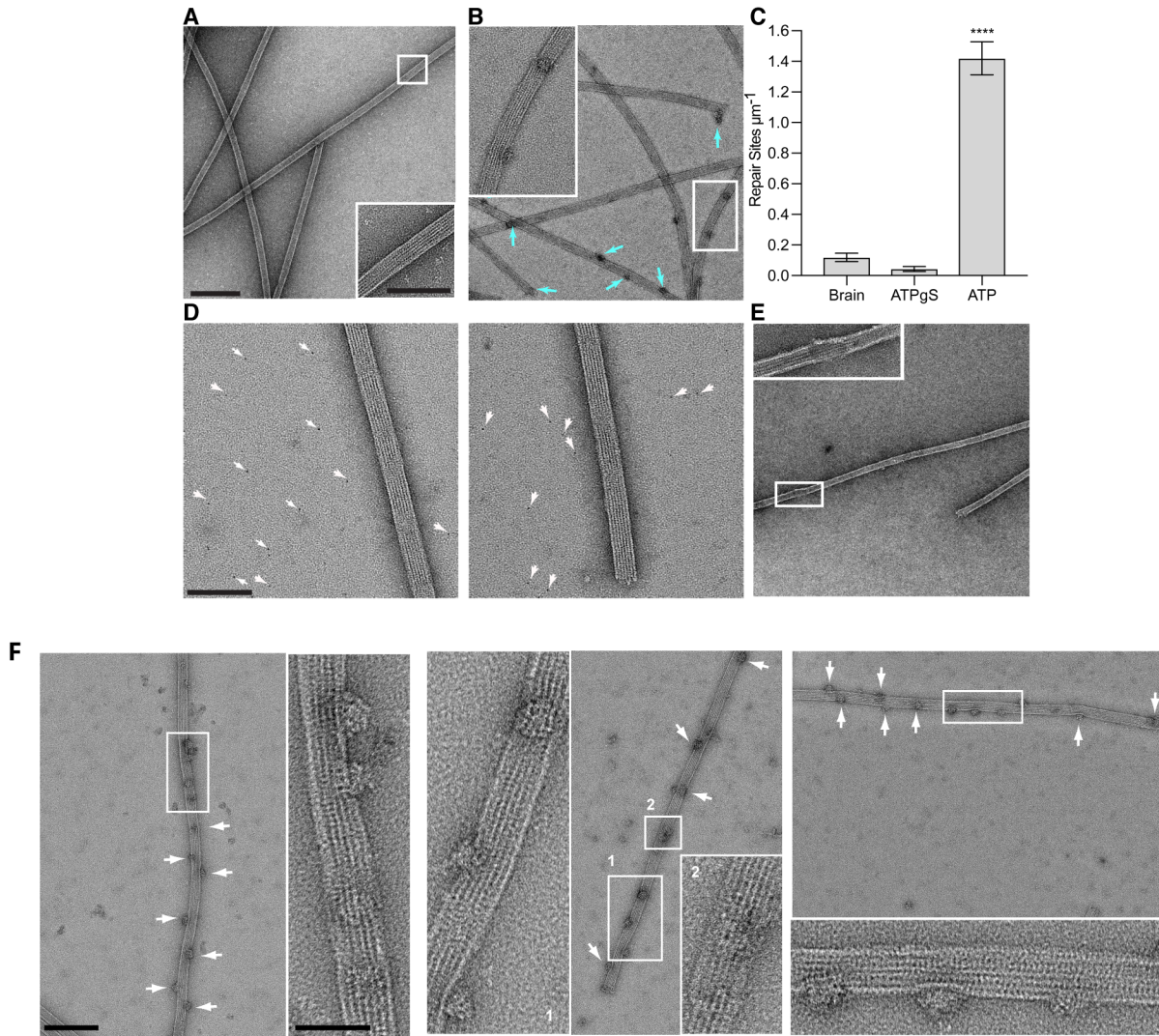


**Fig. S7.**

**TEM shows tubulin incorporates productively into microtubules at nanoscale damage sites.**

(A, B) Fields of GMPCPP brain microtubules damaged with spastin at the nanoscale and repaired with FLAG-tagged recombinant human  $\alpha$ 1A/ $\beta$ III tubulin negatively stained and visualized by TEM. Microtubules were incubated with spastin in solution for 30 sec in the presence of ATP $\gamma$ S (A) or ATP (B) and then repaired for 5 min by addition of soluble recombinant FLAG-tagged tubulin. Repair sites detected by anti-FLAG antibodies coupled with gold-conjugated secondary antibodies and are indicated by cyan arrows. Microtubules were imaged at 6,800x, scale bar 250 nm, and 18,500x, scale bar 100 nm, (*insets*) on a T12 Technai electron microscope (FEI) equipped with a 2k x 2k Gatan US1000 CCD camera. (C) Number of gold-conjugated secondary-primary antibody complexes detected on brain microtubules incubated with spastin and brain tubulin in the presence of ATP; brain microtubules incubated with spastin and recombinant tubulin in the presence of ATP $\gamma$ S or ATP. 278 images and 93.7  $\mu\text{m}$  of microtubule lattice, 300 images and 188.4  $\mu\text{m}$  of microtubule lattice and 339 images and 252.9  $\mu\text{m}$  of microtubule lattice were analyzed for the brain tubulin, recombinant tubulin with ATP $\gamma$ S and recombinant tubulin with ATP conditions, respectively. Error bars, s.e.m. \*\*\*\*, P values < 0.0001 determined by

two-tailed t test. **(D)** Immunogold-conjugated secondary antibodies and anti-FLAG antibodies, highlighted by white arrows, do not decorate brain microtubules. Scale bar 100nm. Microtubules imaged at 18,500x magnification, scale bar 100 nm. **(E)** Unrepaired microtubules that were incubated with spastin but not with soluble recombinant tubulin. Microtubules imaged at 6,800x and 18,500x (insets) magnification. **(F)** Nanoscale damage sites repaired with recombinant tubulin visualized at a magnification of 9,600, Scale bar, 200 nm; 50,000 magnification for the insets, Scale bar 50 nm (Materials and methods). Repair sites were detected by anti-FLAG antibodies coupled with gold-conjugated secondary antibodies and are indicated by white arrows. The easy detection of repair sites relied on the high negative stain contrast of the primary and secondary antibodies, together with the contrast contributed by the 4 nm gold particles. Because the antibodies lie in multiple orientations, as the FLAG epitope is in the flexible and easily accessible tubulin tail, the 4 nm gold particles are not concentrated in a tight spot (Materials and methods)

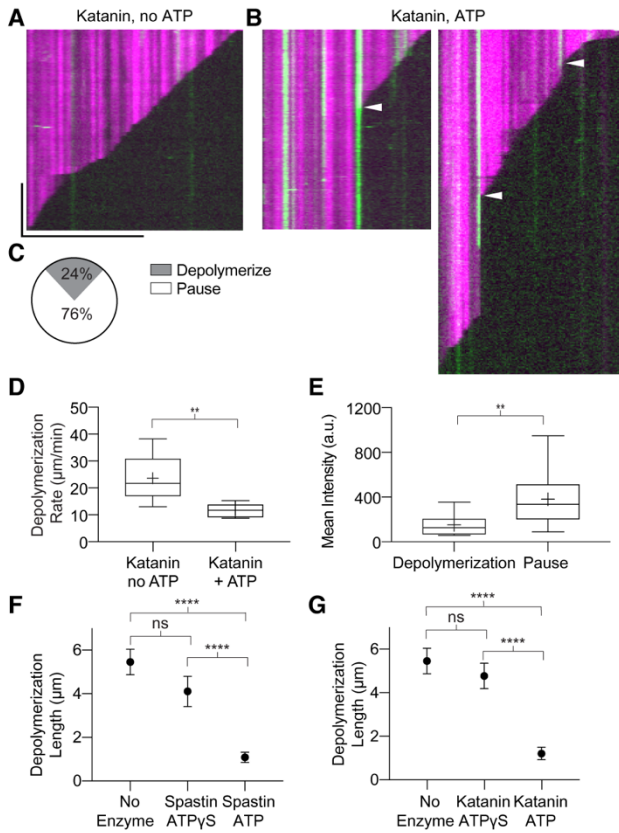


**Fig. S8.**

**Katanin generated GMPCPP-islands protect against depolymerization**

(A, B) Representative kymographs of laser ablated microtubules (magenta) depolymerizing when incubated with katanin, no ATP with no visible GMPCPP-tubulin incorporation (green) (A) or pausing at sites of GMPCPP-tubulin islands introduced by katanin in the presence of ATP (B). White arrows designate pause sites. Horizontal scale bar,  $5\mu\text{m}$  and vertical scale bar, 10 sec. (C) Pie chart shows distribution of GMPCPP tubulin islands where microtubules paused (white) or continued depolymerization (gray) after laser-induced depolymerization;  $n = 37$  GMPCPP tubulin islands from 21 microtubules from multiple chambers. (D) Depolymerization rates of microtubules incubated with katanin, no ATP or through GMPCPP islands for microtubules incubated with katanin, ATP;  $n = 22$  microtubules and 6 microtubules with GMPCPP islands for katanin, no ATP and katanin, ATP, respectively. (E) Mean intensity of GMPCPP islands through which microtubules depolymerized or paused in the katanin, ATP condition;  $n = 11$  and 23 for depolymerization and pauses, respectively. \*\* represents  $P < 0.01$  determined by the Mann-Whitney test. (F, G) Average polymer mass lost per severing-induced depolymerization event at  $12\mu\text{M}$  tubulin in the absence of any enzyme or in the presence of spastin or katanin with  $1\text{mM}$  ATP $\gamma$ S or ATP;  $n = 24$  for no enzyme;  $n = 12$  and 38 for spastin and katanin with ATP $\gamma$ S, respectively;  $n = 25$  and 27 for spastin or katanin with ATP, respectively, all from multiple chambers. Severing was triggered through laser ablation in the no enzyme, or spastin with ATP $\gamma$ S and katanin with ATP $\gamma$ S conditions. ns, not significant; \*\*\*\* represents  $P < 0.0001$  determined by the Mann-Whitney test.

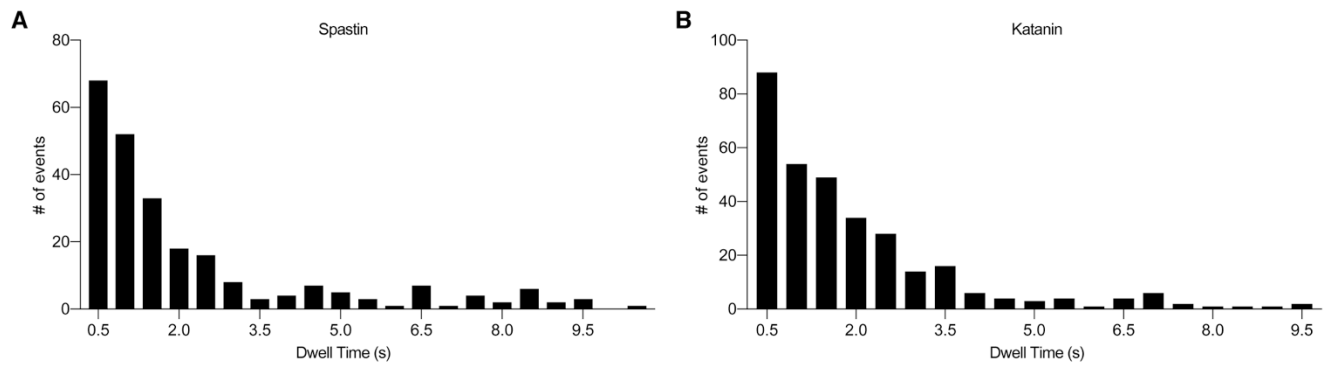


**Fig. S9.**

**Residence times of EB1-GFP lattice puncta**

**(A)** Dwell times of EB1-GFP lattice puncta on dynamic microtubules at 10  $\mu$ M tubulin in the presence of 25 nM spastin and 1mM ATP; n=244. **(B)** Dwell times of EB1-GFP lattice puncta on dynamic microtubules at 10  $\mu$ M tubulin in the presence of 25 nM katanin and 1mM ATP, n=318.



ATP. Fluorescence line scans (bottom panels) along these microtubules showing EB1-GFP and tubulin intensities. Rescue sites are highlighted by yellow arrows and a dotted line. Scale bar, 2  $\mu\text{m}$ .

### **Movie S1.**

#### **Live imaging of spastin induced nanodamage and repair of GMPCPP-capped GDP microtubules.**

GMPCPP-capped GDP microtubules incubated with spastin (5nM) in the absence (left) or presence of 5  $\mu$ M HiLyte488-labeled soluble tubulin (right). Magenta, non-stabilized microtubule segment; bright cyan, GMPCPP tubulin cap; cyan puncta, incorporated HiLyte488-labeled tubulin at nanodamage sites. Repair sites indicated by white arrows, severing sites by yellow arrows. Images acquired at 20 fps and played back at 50 fps. Scale bar, 5  $\mu$ m.

### **Movie S2.**

#### **Live imaging of tubulin incorporation into dynamic microtubules in the presence of spastin.**

12  $\mu$ M 10% HiLyte 647-labeled dynamic microtubules (magenta) imaged as 12 $\mu$ M 10% HiLyte488-labeled tubulin (cyan) is perfused into the chamber together with spastin, no ATP (top) or spastin, ATP (bottom). The HiLyte488-labeled tubulin incorporates at nanoscale damage sites and microtubule tips in the ATP condition and only at the tips in the no ATP condition. White arrows designate repair sites. Images acquired at 2 fps and played back at 10 fps. Scale bar, 5  $\mu$ m.

### **Movie S3.**

#### **Live imaging of tubulin incorporation into dynamic microtubules in the presence of katanin.**

12  $\mu$ M 10% HiLyte 647-labeled dynamic microtubules (magenta) imaged as 12 $\mu$ M 10% HiLyte488-labeled tubulin (cyan) is perfused into the chamber together with katanin, no ATP (top) or katanin, ATP (bottom). The HiLyte488-labeled tubulin incorporates at nanoscale damage sites along the microtubule and microtubule tips in the ATP condition and only at the tips in the no ATP condition. White arrows designate repair sites. Images acquired at 2 fps and played back at 6 fps. Scale bar, 5  $\mu$ m.

### **Movie S4.**

#### **Spastin-generated GMPCPP islands pause depolymerization.**

Depolymerizing laser ablated GDP-microtubules after pre-incubation with spastin, no ATP (top) or spastin, ATP (bottom) in the presence of soluble tubulin with 200  $\mu$ M GMPCPP and washout of the enzymes and soluble tubulin (Materials and methods and Fig. 5A). Magenta, GDP-microtubule; green, GMPCPP-tubulin islands. White arrows designate incorporated GMPCPP-tubulin islands and purple arrow indicates the site of laser ablation. Images were filtered using Smooth filter in Fiji. Images acquired at 3.1 fps and played back at 10 fps. Scale bar, 5  $\mu$ m.

### **Movie S5.**

#### **Rescues at spastin-generated GMPCPP-tubulin islands.**

Complete depolymerization of a laser-ablated GDP-microtubule devoid of GMPCPP-tubulin islands (top) and microtubule rescue at a GMPCPP-tubulin island introduced by spastin in an ATP dependent manner (bottom) (Materials and methods and Fig. 5A). Magenta, GDP-microtubule; green, GMPCPP-tubulin islands. Purple arrow indicates the site of laser ablation, white arrow designates the GMPCPP-tubulin island at the site of rescue and the blue arrow designates the microtubule rescue. Images were filtered using Smooth filter in Fiji. Images acquired at 3.1 fps and played back at 60 fps. Scale bar, 5  $\mu$ m.

### **Movie S6.**

#### **Spastin action recruits EB1 transiently along the microtubule.**

Dynamic microtubules in the presence of EB1-GFP without spastin (top) or after the perfusion of spastin with ATP (bottom). Magenta, HiLyte 647 labeled microtubule; green, EB1-GFP. White arrows designate EB1 recruited to the microtubule lattice, blue arrows designate EB1 recruited at the growing plus ends. Images acquired at 2 fps and played back at 10 fps. Scale bar, 2  $\mu$ m.

**Movie S7.**

**Laser ablated microtubules quickly rescue in the presence of katanin and ATP.**

Laser ablated dynamic microtubules in the presence of EB1-GFP and katanin with 1mM ATP $\gamma$ S (top) or 1mM ATP (bottom). Magenta, HiLyte 647 labeled microtubule; green, EB1-GFP. Images acquired at 2.9 fps and played back at 10 fps.

## References and Notes

1. A. Roll-Mecak, F. J. McNally, Microtubule-severing enzymes. *Curr. Opin. Cell Biol.* **22**, 96–103 (2010). [doi:10.1016/j.ceb.2009.11.001](https://doi.org/10.1016/j.ceb.2009.11.001) [Medline](#)
2. N. T. Sherwood, Q. Sun, M. Xue, B. Zhang, K. Zinn, *Drosophila* spastin regulates synaptic microtubule networks and is required for normal motor function. *PLOS Biol.* **2**, e429 (2004). [doi:10.1371/journal.pbio.0020429](https://doi.org/10.1371/journal.pbio.0020429) [Medline](#)
3. N. Trotta, G. Orso, M. G. Rossetto, A. Daga, K. Broadie, The hereditary spastic paraplegia gene, *spastin*, regulates microtubule stability to modulate synaptic structure and function. *Curr. Biol.* **14**, 1135–1147 (2004). [doi:10.1016/j.cub.2004.06.058](https://doi.org/10.1016/j.cub.2004.06.058) [Medline](#)
4. M. C. Stone, K. Rao, K. W. Gheres, S. Kim, J. Tao, C. La Rochelle, C. T. Folker, N. T. Sherwood, M. M. Rolls, Normal *spastin* gene dosage is specifically required for axon regeneration. *Cell Rep.* **2**, 1340–1350 (2012). [doi:10.1016/j.celrep.2012.09.032](https://doi.org/10.1016/j.celrep.2012.09.032) [Medline](#)
5. F. J. Ahmad, W. Yu, F. J. McNally, P. W. Baas, An essential role for katanin in severing microtubules in the neuron. *J. Cell Biol.* **145**, 305–315 (1999). [doi:10.1083/jcb.145.2.305](https://doi.org/10.1083/jcb.145.2.305) [Medline](#)
6. V. Stoppin-Mellet, J. Gaillard, M. Vantard, Katanin's severing activity favors bundling of cortical microtubules in plants. *Plant J.* **46**, 1009–1017 (2006). [doi:10.1111/j.1365-313X.2006.02761.x](https://doi.org/10.1111/j.1365-313X.2006.02761.x) [Medline](#)
7. Q. Zhang, E. Fishel, T. Bertroche, R. Dixit, Microtubule severing at crossover sites by katanin generates ordered cortical microtubule arrays in *Arabidopsis*. *Curr. Biol.* **23**, 2191–2195 (2013). [doi:10.1016/j.cub.2013.09.018](https://doi.org/10.1016/j.cub.2013.09.018) [Medline](#)
8. J. J. Lindeboom, M. Nakamura, A. Hibbel, K. Shundyak, R. Gutierrez, T. Ketelaar, A. M. C. Emons, B. M. Mulder, V. Kirik, D. W. Ehrhardt, A mechanism for reorientation of cortical microtubule arrays driven by microtubule severing. *Science* **342**, 1245533 (2013). [doi:10.1126/science.1245533](https://doi.org/10.1126/science.1245533) [Medline](#)
9. D. Zhang, G. C. Rogers, D. W. Buster, D. J. Sharp, Three microtubule severing enzymes contribute to the “Pacman-flux” machinery that moves chromosomes. *J. Cell Biol.* **177**, 231–242 (2007). [doi:10.1083/jcb.200612011](https://doi.org/10.1083/jcb.200612011) [Medline](#)
10. K. McNally, A. Audhya, K. Oegema, F. J. McNally, Katanin controls mitotic and meiotic spindle length. *J. Cell Biol.* **175**, 881–891 (2006). [doi:10.1083/jcb.200608117](https://doi.org/10.1083/jcb.200608117) [Medline](#)
11. R. Loughlin, J. D. Wilbur, F. J. McNally, F. J. Nédélec, R. Heald, Katanin contributes to interspecies spindle length scaling in *Xenopus*. *Cell* **147**, 1397–1407 (2011). [doi:10.1016/j.cell.2011.11.014](https://doi.org/10.1016/j.cell.2011.11.014) [Medline](#)
12. K. McNally, E. Berg, D. B. Cortes, V. Hernandez, P. E. Mains, F. J. McNally, Katanin maintains meiotic metaphase chromosome alignment and spindle structure in vivo and has multiple effects on microtubules in vitro. *Mol. Biol. Cell* **25**, 1037–1049 (2014). [doi:10.1091/mbc.e13-12-0764](https://doi.org/10.1091/mbc.e13-12-0764) [Medline](#)
13. N. Sharma, J. Bryant, D. Wloga, R. Donaldson, R. C. Davis, M. Jerka-Dziadosz, J. Gaertig, Katanin regulates dynamics of microtubules and biogenesis of motile cilia. *J. Cell Biol.* **178**, 1065–1079 (2007). [doi:10.1083/jcb.200704021](https://doi.org/10.1083/jcb.200704021) [Medline](#)

14. W. F. Hu, O. Pomp, T. Ben-Omran, A. Kodani, K. Henke, G. H. Mochida, T. W. Yu, M. B. Woodworth, C. Bonnard, G. S. Raj, T. T. Tan, H. Hamamy, A. Masri, M. Shboul, M. Al Saffar, J. N. Partlow, M. Al-Dosari, A. Alazami, M. Alowain, F. S. Alkuraya, J. F. Reiter, M. P. Harris, B. Reversade, C. A. Walsh, Katanin p80 regulates human cortical development by limiting centriole and cilia number. *Neuron* **84**, 1240–1257 (2014). [doi:10.1016/j.neuron.2014.12.017](https://doi.org/10.1016/j.neuron.2014.12.017) [Medline](#)
15. K. Mishra-Gorur, A. O. Çağlayan, A. E. Schaffer, C. Chabu, O. Henegariu, F. Vonhoff, G. T. Akgümüş, S. Nishimura, W. Han, S. Tu, B. Baran, H. Gümüş, C. Dilber, M. S. Zaki, H. A. A. Hossni, J.-B. Rivière, H. Kayserili, E. G. Spencer, R. Ö. Rosti, J. Schroth, H. Per, C. Çağlar, Ç. Çağlar, D. Dölen, J. F. Baranoski, S. Kumandaş, F. J. Minja, E. Z. Erson-Omay, S. M. Mane, R. P. Lifton, T. Xu, H. Keshishian, W. B. Dobyns, N. C. Chi, N. Šestan, A. Louvi, K. Bilgüvar, K. Yasuno, J. G. Gleeson, M. Günel, Mutations in KATNB1 cause complex cerebral malformations by disrupting asymmetrically dividing neural progenitors. *Neuron* **84**, 1226–1239 (2014). [doi:10.1016/j.neuron.2014.12.014](https://doi.org/10.1016/j.neuron.2014.12.014) [Medline](#)
16. J. W. Connell, C. Lindon, J. P. Luzio, E. Reid, Spastin couples microtubule severing to membrane traffic in completion of cytokinesis and secretion. *Traffic* **10**, 42–56 (2009). [doi:10.1111/j.1600-0854.2008.00847.x](https://doi.org/10.1111/j.1600-0854.2008.00847.x) [Medline](#)
17. J. Guizetti, L. Schermelleh, J. Mäntler, S. Maar, I. Poser, H. Leonhardt, T. Müller-Reichert, D. W. Gerlich, Cortical constriction during abscission involves helices of ESCRT-III-dependent filaments. *Science* **331**, 1616–1620 (2011). [doi:10.1126/science.1201847](https://doi.org/10.1126/science.1201847) [Medline](#)
18. A. Karabay, W. Yu, J. M. Solowska, D. H. Baird, P. W. Baas, Axonal growth is sensitive to the levels of katanin, a protein that severs microtubules. *J. Neurosci.* **24**, 5778–5788 (2004). [doi:10.1523/JNEUROSCI.1382-04.2004](https://doi.org/10.1523/JNEUROSCI.1382-04.2004) [Medline](#)
19. R. A. Charafeddine, J. Makdisi, D. Schairer, B. P. O'Rourke, J. D. Diaz-Valencia, J. Chouake, A. Kutner, A. Krausz, B. Adler, P. Nacharaju, H. Liang, S. Mukherjee, J. M. Friedman, A. Friedman, J. D. Nosanchuk, D. J. Sharp, Fidgetin-Like 2: A microtubule-based regulator of wound healing. *J. Invest. Dermatol.* **135**, 2309–2318 (2015). [doi:10.1038/jid.2015.94](https://doi.org/10.1038/jid.2015.94) [Medline](#)
20. G. Yigit, D. Wiczorek, N. Bögershausen, F. Beleggia, C. Möller-Hartmann, J. Altmüller, H. Thiele, P. Nürnberg, B. Wollnik, A syndrome of microcephaly, short stature, polysyndactyly, and dental anomalies caused by a homozygous KATNB1 mutation. *Am. J. Med. Genet. A* **170**, 728–733 (2016). [doi:10.1002/ajmg.a.37484](https://doi.org/10.1002/ajmg.a.37484) [Medline](#)
21. A. Roll-Mecak, R. D. Vale, The *Drosophila* homologue of the hereditary spastic paraplegia protein, spastin, severs and disassembles microtubules. *Curr. Biol.* **15**, 650–655 (2005). [doi:10.1016/j.cub.2005.02.029](https://doi.org/10.1016/j.cub.2005.02.029) [Medline](#)
22. K. Jiang, L. Rezaczkova, S. Hua, Q. Liu, G. Capitani, A. F. M. Altelaar, A. J. R. Heck, R. A. Kammerer, M. O. Steinmetz, A. Akhmanova, Microtubule minus-end regulation at spindle poles by an ASPM-katanin complex. *Nat. Cell Biol.* **19**, 480–492 (2017). [doi:10.1038/ncb3511](https://doi.org/10.1038/ncb3511) [Medline](#)
23. J. D. Wood, J. A. Landers, M. Bingley, C. J. McDermott, V. Thomas-McArthur, L. J. Gleadall, P. J. Shaw, V. T. Cunliffe, The microtubule-severing protein Spastin is essential

- for axon outgrowth in the zebrafish embryo. *Hum. Mol. Genet.* **15**, 2763–2771 (2006).  
[doi:10.1093/hmg/ddl212](https://doi.org/10.1093/hmg/ddl212) [Medline](#)
24. D. H. Burk, Z.-H. Ye, Alteration of oriented deposition of cellulose microfibrils by mutation of a katanin-like microtubule-severing protein. *Plant Cell* **14**, 2145–2160 (2002).  
[doi:10.1105/tpc.003947](https://doi.org/10.1105/tpc.003947) [Medline](#)
  25. M. Srayko, E. T. O’toole, A. A. Hyman, T. Müller-Reichert, Katanin disrupts the microtubule lattice and increases polymer number in *C. elegans* meiosis. *Curr. Biol.* **16**, 1944–1949 (2006). [doi:10.1016/j.cub.2006.08.029](https://doi.org/10.1016/j.cub.2006.08.029) [Medline](#)
  26. K. Ribbeck, T. J. Mitchison, Meiotic spindle: Sculpted by severing. *Curr. Biol.* **16**, R923–R925 (2006). [doi:10.1016/j.cub.2006.09.048](https://doi.org/10.1016/j.cub.2006.09.048) [Medline](#)
  27. A. Roll-Mecak, R. D. Vale, Making more microtubules by severing: A common theme of noncentrosomal microtubule arrays? *J. Cell Biol.* **175**, 849–851 (2006).  
[doi:10.1083/jcb.200611149](https://doi.org/10.1083/jcb.200611149) [Medline](#)
  28. R. A. Walker, S. Inoué, E. D. Salmon, Asymmetric behavior of severed microtubule ends after ultraviolet-microbeam irradiation of individual microtubules in vitro. *J. Cell Biol.* **108**, 931–937 (1989). [doi:10.1083/jcb.108.3.931](https://doi.org/10.1083/jcb.108.3.931) [Medline](#)
  29. P. T. Tran, R. A. Walker, E. D. Salmon, A metastable intermediate state of microtubule dynamic instability that differs significantly between plus and minus ends. *J. Cell Biol.* **138**, 105–117 (1997). [doi:10.1083/jcb.138.1.105](https://doi.org/10.1083/jcb.138.1.105) [Medline](#)
  30. T. Mitchison, M. Kirschner, Dynamic instability of microtubule growth. *Nature* **312**, 237–242 (1984). [doi:10.1038/312237a0](https://doi.org/10.1038/312237a0) [Medline](#)
  31. M. F. Carlier, D. Pantaloni, Kinetic analysis of guanosine 5'-triphosphate hydrolysis associated with tubulin polymerization. *Biochemistry* **20**, 1918–1924 (1981).  
[doi:10.1021/bi00510a030](https://doi.org/10.1021/bi00510a030) [Medline](#)
  32. D. Zhang, K. D. Grode, S. F. Stewman, J. D. Diaz-Valencia, E. Liebling, U. Rath, T. Riera, J. D. Currie, D. W. Buster, A. B. Asenjo, H. J. Sosa, J. L. Ross, A. Ma, S. L. Rogers, D. J. Sharp, *Drosophila* katanin is a microtubule depolymerase that regulates cortical-microtubule plus-end interactions and cell migration. *Nat. Cell Biol.* **13**, 361–370 (2011).  
[doi:10.1038/ncb2206](https://doi.org/10.1038/ncb2206) [Medline](#)
  33. L. Schaedel, K. John, J. Gaillard, M. V. Nachury, L. Blanchoin, M. Théry, Microtubules self-repair in response to mechanical stress. *Nat. Mater.* **14**, 1156–1163 (2015).  
[doi:10.1038/nmat4396](https://doi.org/10.1038/nmat4396) [Medline](#)
  34. C. Aumeier, L. Schaedel, J. Gaillard, K. John, L. Blanchoin, M. Théry, Self-repair promotes microtubule rescue. *Nat. Cell Biol.* **18**, 1054–1064 (2016). [doi:10.1038/ncb3406](https://doi.org/10.1038/ncb3406) [Medline](#)
  35. M. E. Bailey, D. L. Sackett, J. L. Ross, Katanin severing and binding microtubules are inhibited by tubulin carboxy tails. *Biophys. J.* **109**, 2546–2561 (2015).  
[doi:10.1016/j.bpj.2015.11.011](https://doi.org/10.1016/j.bpj.2015.11.011) [Medline](#)
  36. G. Hiller, K. Weber, Radioimmunoassay for tubulin: A quantitative comparison of the tubulin content of different established tissue culture cells and tissues. *Cell* **14**, 795–804 (1978). [doi:10.1016/0092-8674\(78\)90335-5](https://doi.org/10.1016/0092-8674(78)90335-5) [Medline](#)

37. D. N. Itzhak, S. Tyanova, J. Cox, G. H. Borner, Global, quantitative and dynamic mapping of protein subcellular localization. *eLife* **5**, e16950 (2016). [doi:10.7554/eLife.16950](https://doi.org/10.7554/eLife.16950) [Medline](#)
38. A. Vemu, J. Atherton, J. O. Spector, A. Szyk, C. A. Moores, A. Roll-Mecak, Structure and dynamics of single-isoform recombinant neuronal human tubulin. *J. Biol. Chem.* **291**, 12907–12915 (2016). [doi:10.1074/jbc.C116.731133](https://doi.org/10.1074/jbc.C116.731133) [Medline](#)
39. M.-F. Carrier, Guanosine-5'-triphosphate hydrolysis and tubulin polymerization. *Mol. Cell. Biochem.* **47**, 97–113 (1982). [doi:10.1007/BF00234410](https://doi.org/10.1007/BF00234410) [Medline](#)
40. M. F. Carrier, D. Pantaloni, Assembly of microtubule protein: Role of guanosine di- and triphosphate nucleotides. *Biochemistry* **21**, 1215–1224 (1982). [doi:10.1021/bi00535a017](https://doi.org/10.1021/bi00535a017) [Medline](#)
41. M. F. Carrier, D. Didry, D. Pantaloni, Microtubule elongation and guanosine 5'-triphosphate hydrolysis. Role of guanine nucleotides in microtubule dynamics. *Biochemistry* **26**, 4428–4437 (1987). [doi:10.1021/bi00388a036](https://doi.org/10.1021/bi00388a036) [Medline](#)
42. V. VanBuren, D. J. Odde, L. Cassimeris, Estimates of lateral and longitudinal bond energies within the microtubule lattice. *Proc. Natl. Acad. Sci. U.S.A.* **99**, 6035–6040 (2002). [doi:10.1073/pnas.092504999](https://doi.org/10.1073/pnas.092504999) [Medline](#)
43. A. Dimitrov, M. Quesnoit, S. Moutel, I. Cantaloube, C. Poüs, F. Perez, Detection of GTP-tubulin conformation in vivo reveals a role for GTP remnants in microtubule rescues. *Science* **322**, 1353–1356 (2008). [doi:10.1126/science.1165401](https://doi.org/10.1126/science.1165401) [Medline](#)
44. J. Al-Bassam, H. Kim, G. Brouhard, A. van Oijen, S. C. Harrison, F. Chang, CLASP promotes microtubule rescue by recruiting tubulin dimers to the microtubule. *Dev. Cell* **19**, 245–258 (2010). [doi:10.1016/j.devcel.2010.07.016](https://doi.org/10.1016/j.devcel.2010.07.016) [Medline](#)
45. K. Ichihara, H. Kitazawa, Y. Iguchi, H. Hotani, T. J. Itoh, Visualization of the stop of microtubule depolymerization that occurs at the high-density region of microtubule-associated protein 2 (MAP2). *J. Mol. Biol.* **312**, 107–118 (2001). [doi:10.1006/jmbi.2001.4934](https://doi.org/10.1006/jmbi.2001.4934) [Medline](#)
46. M. Zanic, J. H. Stear, A. A. Hyman, J. Howard, EB1 recognizes the nucleotide state of tubulin in the microtubule lattice. *PLOS ONE* **4**, e7585 (2009). [doi:10.1371/journal.pone.0007585](https://doi.org/10.1371/journal.pone.0007585) [Medline](#)
47. S. P. Maurer, F. J. Fourniol, G. Bohner, C. A. Moores, T. Surrey, EBs recognize a nucleotide-dependent structural cap at growing microtubule ends. *Cell* **149**, 371–382 (2012). [doi:10.1016/j.cell.2012.02.049](https://doi.org/10.1016/j.cell.2012.02.049) [Medline](#)
48. T. P. Spurck, O. G. Stonington, J. A. Snyder, J. D. Pickett-Heaps, A. Bajer, J. Mole-Bajer, UV microbeam irradiations of the mitotic spindle. II. Spindle fiber dynamics and force production. *J. Cell Biol.* **111**, 1505–1518 (1990). [doi:10.1083/jcb.111.4.1505](https://doi.org/10.1083/jcb.111.4.1505) [Medline](#)
49. J. Brugués, V. Nuzzo, E. Mazur, D. J. Needleman, Nucleation and transport organize microtubules in metaphase spindles. *Cell* **149**, 554–564 (2012). [doi:10.1016/j.cell.2012.03.027](https://doi.org/10.1016/j.cell.2012.03.027) [Medline](#)
50. R. B. Nicklas, G. M. Lee, C. L. Rieder, G. Rupp, Mechanically cut mitotic spindles: Clean cuts and stable microtubules. *J. Cell Sci.* **94**, 415–423 (1989). [Medline](#)

51. J. S. Tirnauer, E. D. Salmon, T. J. Mitchison, Microtubule plus-end dynamics in *Xenopus* egg extract spindles. *Mol. Biol. Cell* **15**, 1776–1784 (2004). [doi:10.1091/mbc.e03-11-0824](https://doi.org/10.1091/mbc.e03-11-0824) [Medline](#)
52. J. Howard, A. A. Hyman, Microtubule polymerases and depolymerases. *Curr. Opin. Cell Biol.* **19**, 31–35 (2007). [doi:10.1016/j.ceb.2006.12.009](https://doi.org/10.1016/j.ceb.2006.12.009) [Medline](#)
53. R. D. Vale, Severing of stable microtubules by a mitotically activated protein in *Xenopus* egg extracts. *Cell* **64**, 827–839 (1991). [doi:10.1016/0092-8674\(91\)90511-V](https://doi.org/10.1016/0092-8674(91)90511-V) [Medline](#)
54. M. E. Bailey, M. M. Morelli, J. D. Diaz, J. L. Ross, Katanin P60 targets microtubules with defects. *Biophys. J.* **102**, 701a (2012). [doi:10.1016/j.bpj.2011.11.3806](https://doi.org/10.1016/j.bpj.2011.11.3806)
55. H. de Forges, A. Pilon, I. Cantaloube, A. Pallandre, A.-M. Haghiri-Gosnet, F. Perez, C. Poüs, Localized mechanical stress promotes microtubule rescue. *Curr. Biol.* **26**, 3399–3406 (2016). [doi:10.1016/j.cub.2016.10.048](https://doi.org/10.1016/j.cub.2016.10.048) [Medline](#)
56. C. Wang, W. Liu, G. Wang, J. Li, L. Dong, L. Han, Q. Wang, J. Tian, Y. Yu, C. Gao, Z. Kong, KTN80 confers precision to microtubule severing by specific targeting of katanin complexes in plant cells. *EMBO J.* **36**, 3435–3447 (2017). [doi:10.15252/embj.201796823](https://doi.org/10.15252/embj.201796823) [Medline](#)
57. M. L. Valenstein, A. Roll-Mecak, Graded control of microtubule severing by tubulin glutamylation. *Cell* **164**, 911–921 (2016). [doi:10.1016/j.cell.2016.01.019](https://doi.org/10.1016/j.cell.2016.01.019) [Medline](#)
58. B. Lacroix, J. van Dijk, N. D. Gold, J. Guizetti, G. Aldrian-Herrada, K. Rogowski, D. W. Gerlich, C. Janke, Tubulin polyglutamylation stimulates spastin-mediated microtubule severing. *J. Cell Biol.* **189**, 945–954 (2010). [doi:10.1083/jcb.201001024](https://doi.org/10.1083/jcb.201001024) [Medline](#)
59. T. Nakata, S. Niwa, Y. Okada, F. Perez, N. Hirokawa, Preferential binding of a kinesin-1 motor to GTP-tubulin-rich microtubules underlies polarized vesicle transport. *J. Cell Biol.* **194**, 245–255 (2011). [doi:10.1083/jcb.201104034](https://doi.org/10.1083/jcb.201104034) [Medline](#)
60. A. Y. Chan, M. Bailly, N. Zebda, J. E. Segall, J. S. Condeelis, Role of cofilin in epidermal growth factor-stimulated actin polymerization and lamellipod protrusion. *J. Cell Biol.* **148**, 531–542 (2000). [doi:10.1083/jcb.148.3.531](https://doi.org/10.1083/jcb.148.3.531) [Medline](#)
61. V. DesMarais, M. Ghosh, R. Eddy, J. Condeelis, Cofilin takes the lead. *J. Cell Sci.* **118**, 19–26 (2005). [doi:10.1242/jcs.01631](https://doi.org/10.1242/jcs.01631) [Medline](#)
62. N. E. Ziólkowska, A. Roll-Mecak, In vitro microtubule severing assays. *Methods Mol. Biol.* **1046**, 323–334 (2013). [doi:10.1007/978-1-62703-538-5\\_19](https://doi.org/10.1007/978-1-62703-538-5_19) [Medline](#)
63. E. Zehr, A. Szyk, G. Piszczek, E. Szczesna, X. Zuo, A. Roll-Mecak, Katanin spiral and ring structures shed light on power stroke for microtubule severing. *Nat. Struct. Mol. Biol.* **24**, 717–725 (2017). [doi:10.1038/nsmb.3448](https://doi.org/10.1038/nsmb.3448) [Medline](#)
64. A. J. Albee, C. Wiese, *Xenopus* TACC3/maskin is not required for microtubule stability but is required for anchoring microtubules at the centrosome. *Mol. Biol. Cell* **19**, 3347–3356 (2008). [doi:10.1091/mbc.e07-11-1204](https://doi.org/10.1091/mbc.e07-11-1204) [Medline](#)
65. C. Gell, C. T. Friel, B. Borgonovo, D. N. Drechsel, A. A. Hyman, J. Howard, “Purification of tubulin from porcine brain,” in *Microtubule Dynamics: Methods and Protocols*, A. Straube, Ed. (Springer, 2011), pp. 15–28.

66. A. D. Edelstein, M. A. Tsuchida, N. Amodaj, H. Pinkard, R. D. Vale, N. Stuurman, Advanced methods of microscope control using  $\mu$ Manager software. *J. Biol. Methods* **1**, e10 (2014). [doi:10.14440/jbm.2014.36](https://doi.org/10.14440/jbm.2014.36) [Medline](#)
67. I. R. Gibbons, E. Fronk, A latent adenosine triphosphatase form of dynein 1 from sea urchin sperm flagella. *J. Biol. Chem.* **254**, 187–196 (1979). [Medline](#)

## Severing enzymes amplify microtubule arrays through lattice GTP-tubulin incorporation

Annapurna Vemu, Ewa Szczesna, Elena A. Zehr, Jeffrey O. Spector, Nikolaus Grigorieff, Alexandra M. Deaconescu and Antonina Roll-Mecak

*Science* **361** (6404), eaau1504.  
DOI: 10.1126/science.aau1504

### Severing to build microtubules

Microtubules are essential intracellular polymers, built from tubulin subunits, that establish cell shape, move organelles, and segregate chromosomes during cell division. Vemu *et al.* show that microtubule-severing enzymes extract tubulin subunits along the microtubule shaft. This nanoscale damage is repaired by the incorporation of free tubulin, which stabilizes the microtubule against depolymerization. When extraction outpaces repair, microtubules are severed, emerging with stabilized ends composed of fresh tubulin. The severed microtubules act as templates for new microtubule growth, leading to amplification of microtubule number and mass. Thus, seemingly paradoxically, severing enzymes can increase microtubule mass in processes such as neurogenesis and mitotic spindle assembly.

*Science*, this issue p. eaau1504

#### ARTICLE TOOLS

<http://science.sciencemag.org/content/361/6404/eaau1504>

#### SUPPLEMENTARY MATERIALS

<http://science.sciencemag.org/content/suppl/2018/08/22/361.6404.eaau1504.DC1>

#### REFERENCES

This article cites 66 articles, 24 of which you can access for free  
<http://science.sciencemag.org/content/361/6404/eaau1504#BIBL>

#### PERMISSIONS

<http://www.sciencemag.org/help/reprints-and-permissions>

Use of this article is subject to the [Terms of Service](#)